Calibration Methods
for a Distillation Column
for the XENON1T
Dark Matter Experiment

Kalibrationsmethoden für die Destillationssäule
des Experimentes zur Suche nach Dunkler Materie XENON1T

Bachelor-Arbeit
vorgelegt von: Martin Schlak
September 2012

Institut für Kernphysik
Westfälische Wilhelms-Universität Münster
Gutachter: Prof. Dr. Christian Weinheimer
Zweitgutachter: Prof. Dr. Alfons Khoukaz

WESTFÄLISCHE
WILHELMS-UNIVERSITÄT
MÜNSTER

Abstract

In the last decades, particle physicists have successfully described the properties of all so far known elementary particles in the standard model. But there is strong evidence that only about 5 % of the energy of the universe is compounded by the elementary particles so far known. The rest is supposed to consist of dark matter and dark energy. It has been argued that dark matter are weakly interacting massive particles (WIMP). One candidate for the WIMP is the neutralino predicted by the supersymmetric theory, which goes beyond the standard model.

If the theoretical predictions turn out to be true, our atmosphere must be full of WIMPs. However they are very hard to detect as they are conceived to be particles without charge and only weakly interacting with other particles. Several experiments all over the world try to find WIMPs either in a direct or in an indirect way. One of them is the XENON experiment which aims at a direct detection of WIMPs by their interactions with xenon in a time projection chamber. If the WIMPs interact with xenon, an electron and scintillation light is produced. The light is detected by photomultiplier tubes. The electron is drifted into the gaseous xenon at the top of the time projection chamber where a secondary scintillation process takes place. For this purpose the xenon has to be as pure as possible since electronegative impurities reduce the sensitivity of the detector. Furthermore, radioactive impurities like the isotope ^{85}Kr produce an intrinsic background. The XENON100 experiment has recently been analyzed after it had run 225 days in the Laboratori Nazionali del Gran Sasso (LNGS) in Italy, resulting in the world-best limit of spin-indepedent cross section of WIMP-nucleon scattering [Apr12c]. The successor XENON1T (XENON One Ton) is at the moment being designed and partially built up.

The Münster group of Prof. Dr. Christian Weinheimer is tasked to develop and construct a distillation column for the experimental setup of the XENON1T experiment in the LNGS which is able to purify the xenon from the troublesome isotope ^{85}Kr whose decay—if not removed—superimposes on the WIMP interactions. However it remains a problem how very small krypton concentrations in xenon (in the order of magnitude of parts per trillion, ppt) can be measured to calibrate the distillation column and survey the correct functioning. One promising attempt is the use of a residual gas analyzer (RGA) whose sensitivity is improved by a cold trap. With this method, concentrations of 100 ppt have already been measured in Münster [Ket12]. However, further enhancement is needed to fulfil the requirements for using the system as a calibration tool for the distillation column, on the one hand in sensitivity, on the other hand concerning the handling of the setup. As a project for this bachelor thesis, the setup has been modified to provide an user-friendly stand-alone analyzer for gas analysis at XENON100 and XENON1T.

Contents

CHAPTER 1

Introduction

In this chapter, a theoretical introduction into the concept of dark matter is given and its main properties are discussed. This leads to a description of the way the XENON100 experiment tries to detect dark matter particles and how the successor experiment XENON1T aims for better sensitivity. At the end of this chapter, the project of this bachelor thesis within the XENON1T experiment is motivated.

1.1 Dark matter

Observations about the universe give rise to the hypothesis that the baryonic mass comprises only about 4.5 % of the total energy of the universe whereas the main parts are constituted by dark energy (72 %) and dark matter (23 %).

One of the first evidences for dark matter was the application of Newton's gravitational law to galactic dynamics. From an equilibrium of the gravitational and the centripetal force it follows that

$$\begin{aligned} F_g &= F_c && (1.1) \\ \Rightarrow G\frac{Mm}{r^2} &= \frac{m \cdot v^2}{r} && (1.2) \\ \Leftrightarrow v &\propto \frac{1}{\sqrt{r}} && (1.3) \end{aligned}$$

where v is the velocity of the clouds of neutral hydrogen and r is the radius from the centre. The equation predicts that the velocity of clouds with the same density within a galaxy should decrease with the square root of the distance. However, in known spiral galaxies v does not depend on r for large distances from the galactic center but the value is constant. This is especially striking as the luminous mass in spiral galaxies decreases with a growing radius. This is exemplified for the spiral galaxy NGC 6503 in figure 1.1.

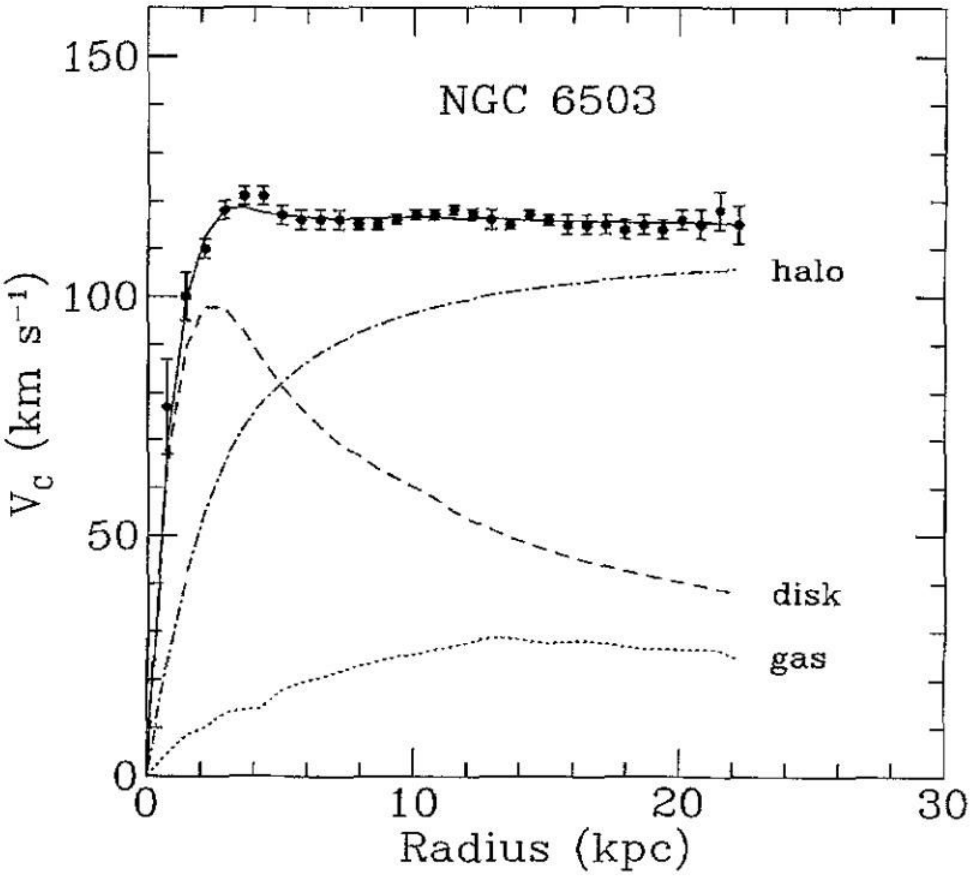

Figure 1.1: **Rotation curve for the spiral galaxy NGC 6503.** The circular rotation velocity remains constant for large radius. To explain this fact, a halo of dark matter is introduced [Beg91].

The contradiction is solved by introducing dark matter. From the measurements, “one infers a galactic dark halo of mass 3-10 times that of the luminous component” [Jun96]. There are further evidences for dark matter such as the cosmic microwave background radiation whose measurements resulted in the matter distribution mentioned above.

It is not yet known what dark matter is made of. Only a small part has been identified as neutrinos, intergalactic gas and supermassive black holes. The main part is supposed to be cold dark matter (CDM).

In the following, the essential properties of CDM are discussed. First of all, “cold” refers to the fact that the particles are non relativistic. Their lifetime is estimated to be greater than the age of the universe, therefore they are stable particles. In addition, CDM particles are neutral [Ost03] and thus do not interact electromagnetically. Dark matter is nonluminous, that means that it neither emits nor absorbs light of any wavelength. Furthermore, CDM is gravitationally self-attractive and clusters with ordinary matter.

One class of particles that fulfil these conditions are weakly interacting massive particles (WIMP) which have a weak scale interaction with ordinary matter [Jun96].

In the theory of supersymmetry which goes beyond the standard model, a particle arises that could be identical with the WIMP. Supersymmetry assigns a new particle to each elementary particle of the standard model, a fermion to a boson and vice versa. As assumed by this theory, supersymmetry was spontaneously broken a few instants after the Big Bang. That is why particles and their supersymmetric twins can have different mass. Most of the supersymmetric particles have very little lifetimes. In the so called minimal supersymmetric model, only the lightest particle called neutralino is stable due to symmetrical considerations (conservation of R-parity). The mass of the neutralino is supposed to be of about 100 GeV and thus in the order of magnitude of the dark matter particle.

1.2 The XENON experiment

Taking into account that WIMPs hardly interact and hence have a very small cross section of $\sigma_\chi \lesssim 10^{-44}$ cm^2 [Apr12c], the detection poses major problems to particle physicists. Two classes of experiments exist: Direct detection experiments search for interactions of dark matter with ordinary matter. On the contrary, indirect detection experiments look for products of WIMP annihilation processes such as electrons, muons and protons in cosmic rays.

The XENON experiment aims at directly detecting WIMPs by their interaction with xenon atoms through a nuclear recoil. The first experiment of the XENON family was XENON10. But the setup has turned out to be too less sensitive to detect dark matter. The successor, XENON100 uses one order of magnitude more xenon as detection material ($\approx$ 62 kg). However, after 225 days of run dark matter has not been found. At the moment the next generation of the XENON experiment, the XENON1T is being built up which again increases the detection mass by one order of magnitude.

In this chapter, we consider the advantages of xenon for dark matter detection first. Subsequently, the design of the experiment is explained.

1.2.1 Xenon as a target material for dark matter detection

Noble liquids like argon and xenon are on the one hand good scintillators and on the other hand good ionizers [Apr10a]. The incoming particle can ionize or only excite the xenon. The excitation process is the following:

$$\begin{aligned} \mathrm{Xe}^* + \mathrm{Xe} + \mathrm{Xe} &\rightarrow \mathrm{Xe}_2^* + \mathrm{Xe} \\ \mathrm{Xe}_2^* &\rightarrow 2\mathrm{Xe} + hv. \end{aligned} \tag{1.4}$$

During this process, the xenon dimer (a molecule of two xenon atoms) emits a vacuum-ultraviolet photon with a wavelength of $\lambda = 178$ nm. Scintillation can also take place after the ionization of xenon:

$$\begin{aligned} \mathrm{Xe}^+ + \mathrm{Xe} &\to \mathrm{Xe}_2^+ \\ \mathrm{Xe}_2^+ + e^- &\to \mathrm{Xe}^{**} + \mathrm{Xe} \\ \mathrm{Xe}^{**} &\to \mathrm{Xe}^* + \mathrm{heat} \\ \mathrm{Xe}^* + \mathrm{Xe} + \mathrm{Xe} &\to \mathrm{Xe}_2^* + \mathrm{Xe} \\ \mathrm{Xe}_2^* &\to 2\mathrm{Xe} + hv. \end{aligned} \tag{1.5}$$

After the ionization process, the xenon recombines with an electron and becomes excited. In the xenon experiment, an electric field is applied to suppress recombination and drift some of the electrons towards the top of the detector. Shortly after the recombination, the xenon atom emits heat via a non-radiative transition [Apr10a]. Subsequently, the scintillation process occurs. This property is exploited by the XENON experiment to detect two independent signals of the nuclear recoil which are used to locate the interaction in space and time. Besides, the two events allow to distinguish the nuclear recoil caused by WIMPs from electronic recoil caused by radioactive radiation. Furthermore, the fact that xenon has odd and even isotopes allows to get a spin independent and spin dependent WIMP-nucleon scattering cross section.

In addition, xenon has the advantage to be a very pure element which naturally does not have long lived radioactives isotopes (besides ^{136}Xe which has a half time of $\tau \approx 2.11 \cdot 10^{21}$ a and thus is not problematic). Another useful property of xenon is its high atomic number ($Z = 54$). That is why xenon is a very heavy element ($\rho_{\mathrm{liquid}} \approx 3$ g/cm^3) and has a self-shielding faculty which protects against radiation coming from outside.

1.2.2 The XENON100 experiment

The core of the XENON100 experiment is a dual phase time projection chamber (TPC) which contains about 62 kg of xenon in a liquid and gaseous phase as a detector material for dark matter (figure 1.2). On the top and bottom of the chamber, photomultiplier tubes (PMT) are installed. An electric field with parallel field lines points downwards. If a xenon atom is ionized, the electron is drifted upwards by the electric field and then extracted into the gas phase at the top. There it is accelerated and causes another scintillation flash S2 which is detected by the PMT. The scintillation photon S1 of the original interaction is detected by the PMT at the bottom and top as well. The sides of the TPC are made of an almost ideal reflector (teflon) to prevent the photon from being absorbed. From the time delay between the two scintillation lights and the drift velocity of the electron, the z-coordinate of the interaction can be located. The hit pattern of the PMT array at the top delivers the x-y-position. This allows a three dimensional reconstruction of the interaction which is necessary to exclude events in the area near the sides where the self-shielding of the xenon is not yet strong enough. Additionally, the ratio of the shapes S1 and S2 allows to distinguish between an electronic and a nuclear recoil. This fact is used for background discrimination.

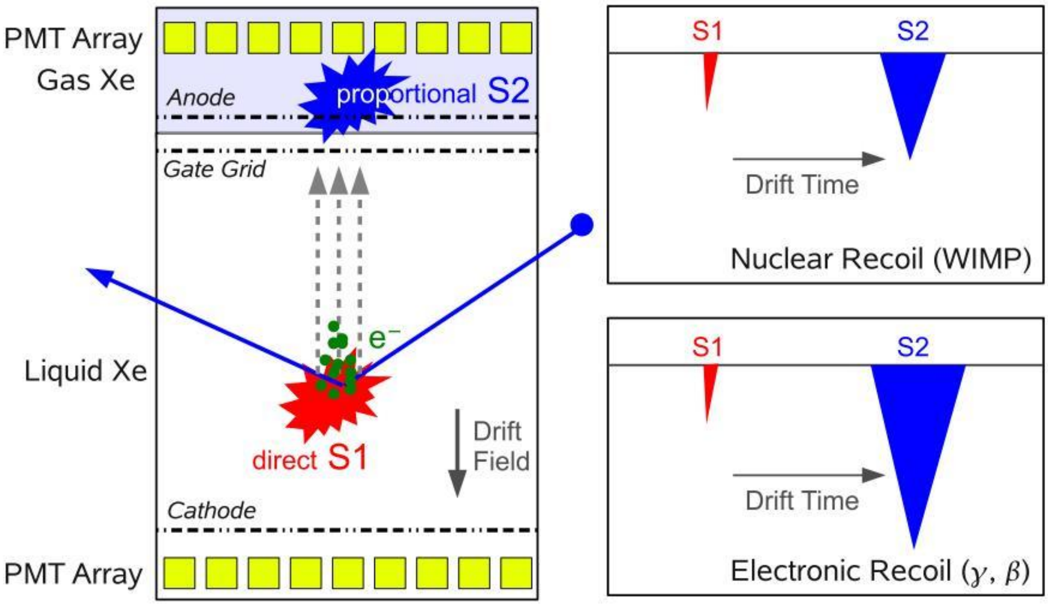

Figure 1.2: **The time projection chamber and discrimination of background events.** The schematic sketch of the time projection chamber (TPC) on the left shows how events are detected. When a WIMP scatters with a xenon atom (nuclear recoil), both scintillation light S1 and ionization occur. The light is measured by a photomultiplier (PMT) in the array on the top or on the bottom. The charge is drifted by an electric field and goes up where it enters in the gaseous xenon and is accelerated again in order to react with the xenon. The second scintillation light caused by this interacting reaches the upper PMT array with a time delay almost equal to the drift time of the electron. On the right, the shapes for the scintillation lights due to nuclear and electronic recoil are compared. Since they are different, a background discrimination is possible [Apr12b].

1.2.3 Results of the XENON100 experiment

The XENON100 experiment has recently been analyzed after it had run 225 days [Apr12c]. The target mass of liquid xenon was 62 kg. The search region for the WIMP particle begins at 6.6 keV_{nr} and is limited to 30.5 keV_{nr}; keV_{nr} is the nuclear equivalent energy scale. Two events in the relevant energy range have been detected, with 1 ± 0.2 expected background events (nuclear recoil and electronic recoil). The probability for two background events in the benchmark region is 26.4 % and thus too high to conclude that WIMPs have been found. However, the results lead to an exclusion limit for the spin-independent WIMP-nucleon cross section σ_χ for $m_\chi > 8$ GeV/c^2 with a minimum at $\sigma_\chi = 2.0 \cdot 10^{-45}$ cm^2 at $m_\chi = 55$ GeV/c^2 (90 % confidence level).

In figure 1.3, this exclusion limit is compared to those of other dark matter detection

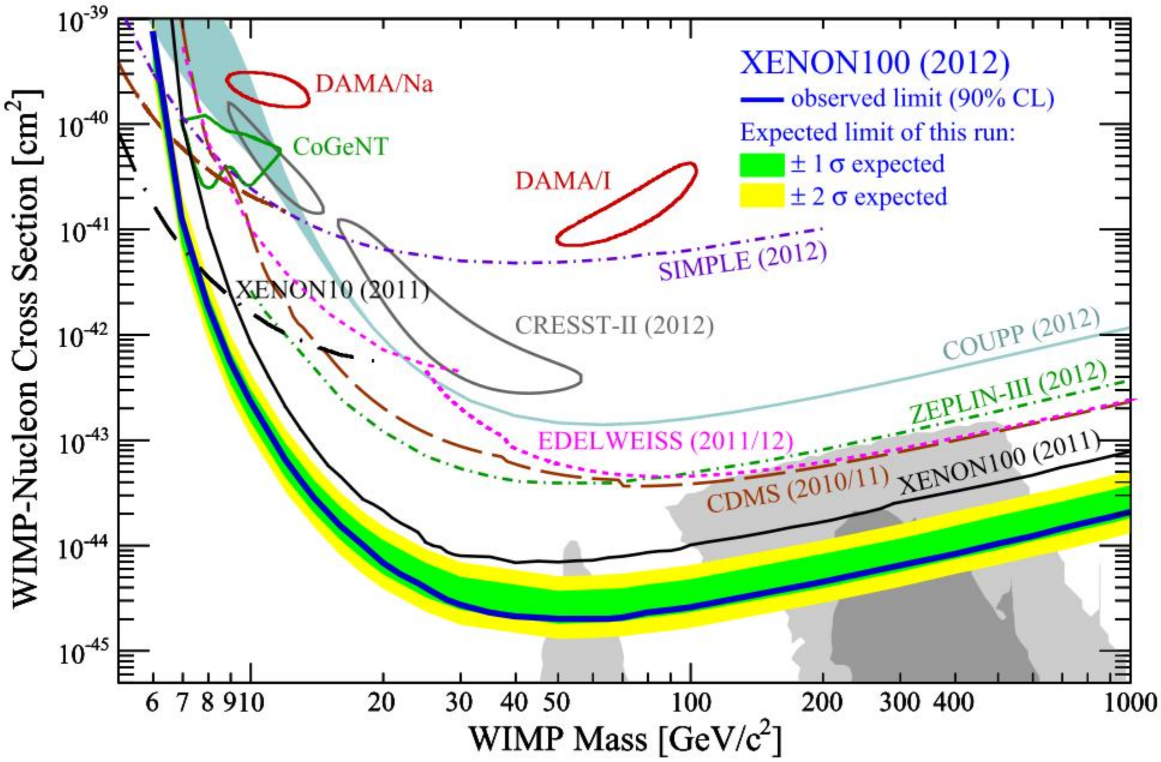

Figure 1.3: **Dark matter nucleus cross sections of different experiments.** The blue line represents the spin-independent cross section exclusion limit of the XENON100 experiment after it have run 225 days. The sensitivity of the XENON100 experiment is greater than those of other dark matter search experiments. Besides, the results challenge other experiments like DAMA which suppose to have found WIMP-nucleon scattering events with cross section up to five orders of magnitude larger [Apr12c].

exclusion limits or calculated cross sections (in the case of the DAMA experiment). It can be inferred that the xenon is the world's most sensitive experiment and challenges the results from other groups. From the results, one can also infer that the reduction of background events is essential for the XENON1T experiment to reach a more confident discrimination between background events and events caused by dark matter.

1.2.4 The XENON1T experiment

The promising data of the XENON100 experiment give rise to the hypothesis that the design of the experiment is successful, however the sensitivity is not yet high enough to detect WIMPs. In the next generation of the XENON experiment, the XENON1T, one aims at a sensitivity for the spin independent cross section of

$$\sigma_\chi = 10^{-47}\,\mathrm{cm}^2 \tag{1.6}$$

by 2015 [Apr10b]. The detection principle in the time projection chamber remains the same with the difference that about 1 t of fiducial target mass are used in the chamber. Additionally, it is taken more care to reduce background events in the time projection chamber. In the following section, the need for a reduction of background events is discussed in more detail.

1.3 Radioactive background

For WIMPs moving with 270 km/s and a mass in the range of 20-400 GeV in the dark halo of our system, the expected rate in the detector can be estimated to 10^{-4} to 1 event per day per kilogram of detector material. During these interactions an energy of 1-100 keV is deposited [Jun96]. This event rate is by far outnumbered by interactions due to cosmic rays, radioactive elements in the underground laboratory and the instruments and intrinsic impurities of the xenon if one does not highly reduce background events. In the XENON100 experiment, background of electronic recoil could be reduced to $5{\cdot}10^{-3}$ events/(keV·kg·day) [Apr12c]. However, for the XENON1T the background should be further reduced by two orders of magnitude.

1.3.1 Shielding against cosmic rays and other radioactive elements

By active and passive shielding, the radioactive background in the time projection chamber is reduced to a minimum. The effects of cosmic rays are reduced by the location of the Laboratori Nazionali del Gran Sasso (LNGS). The thick rock of the Gran Sasso suppresses the cosmic muons flux by a factor 10^6. This is equivalent to a depth in water of 3600 m [Agl98].

Active shielding is enhanced by a water tank with a thickness of about 5 m in all directions around the xenon cryostat which contains the TPC. This shield reduces the neutron flux which is produced by muons in the rock by 99.7 % [Apr10b]. Gamma radiation is also stopped by this shield. A careful selection of radiopure materials used in the xenon cryostat further reduces the background [Apr10b].

In the TPC, the self-shielding faculty of xenon is exploited by doing a “fiducial cut of 10 cm on all side” [Apr10b]. Interactions in the regions close to the sides, which are very likely caused by background effects, are not considered in the dark matter search.

1.3.2 Contamination with krypton

Trace radioactive impurities in the xenon itself constitute an irreducible background. In particular, xenon always contains krypton because it is contracted out of air, which is composed of these two noble gases (among others). Krypton on the other hand has the radioactive isotope ^{85}Kr which is artificially produced in nuclear fission [Abe11]. Although

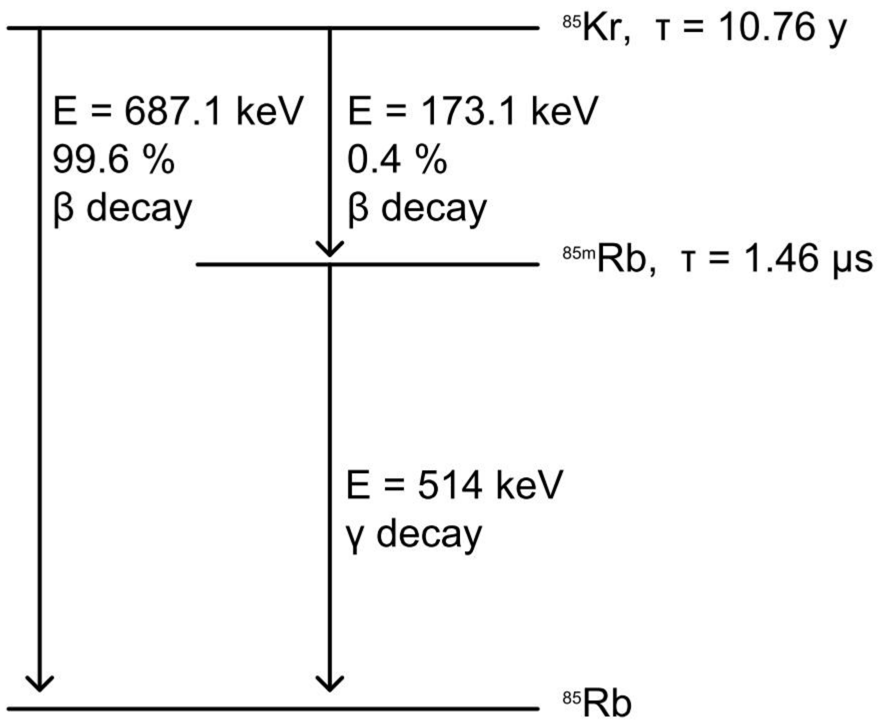

Figure 1.4: **Decay of the krypton isotope ^{85}Kr.** The isotope ^{85}Kr decays with a 99.6 % propability into ^{85}Rb through β decay and with a 0.4 % probability at first into $^{85\mathrm{m}}$Rb through β decay and then into the stable isotope ^{85}Rb through γ decay.

the concentration of $2{\cdot}10^{-11}$ mol/mol (^{85}Kr/$^{\mathrm{nat}}$Kr) is very low, the background rate caused by the β decay of ^{85}Kr is too high for dark matter experiments. As ^{85}Kr has a half-life of 10.76 years, waiting for the ^{85}Kr to decay cannot be the solution either.

^{85}Kr decays with a probability of 99.6 % into the stable isotope ^{85}Rb releasing an energy of 687 keV. It has a 0.4 % branching ratio to decay first to ^{85m}Rb through β decay and then to ^{85}Rb through γ decay (figure 1.4). The intermediate state has a lifetime of 1.46 μs [Apr12b]. In principle, this time delay can be used to measure krypton concentrations. However, in this thesis another method will be employed, namely mass spectrometry enhanced by a cold trap (chapter 2).

The contamination with krypton is especially problematic since neither can it be removed with chemical processes nor are the electrons produced by the β decay shielded by xenon [Dob11]. In order to reduce the krypton concentration from about 10^{-9} mol/mol ($^{\mathrm{nat}}$Kr/Xe) to less than 10^{-12} mol/mol (ppt level), the Münster group is constructing a cryogenic distillation column which prepares the xenon for the dark matter search. This method exploits the fact that the boiling point of liquid krypton is at 120 K, while that of xenon is at 165 K. The purified xenon is gathered at the bottom whereas the xenon with a high concentration of krypton leaves the system at the top of the column.

1.4 Motivation for this thesis

To calibrate the distillation column, the krypton concentration in xenon must be constantly monitored. Furthermore, a monitoring of krypton is needed to find the optimal functional parameters for the distillation column and to better understand the distillation process of xenon. For concentrations of the ppt level, the distillation process has not yet been theoretically investigated.

This monitoring requires a sensitivity down to the ppt level. Standard mass spectrometers cannot measure such low concentrations. But it has been shown that the sensitivity of a residual gas analyzer (RGA) can be enhanced by pumping the gas through a cold trap first. The theoretical details of this method are developped in chapter 2.

In a test setup in Münster of the mass spectrometry enhanced by a cold trap, a sensitivity of 100 ppt has been reached (chapter 3.2). For more details compare [Ket12]. In order to calibrate the distillation column, this value has to be further reduced by at least two orders of magnitude. Therefore, the mass spectrometer and the cold trap have been installed at the main setup in the XENON laboratory in Münster and provided with a butterfly valve that allows a better control of the flow rate through the main chamber with the mass spectrometer.

Another enhancement concernes the handling of the krypton detection setup which constitutes the main task of this bachelor project. In the test setup, a bellow hand valve was used to control the incoming pressure. This is not very user-friendly as it requires constant surveillance and manipulation by the experimenter. Furthermore, results are hardly reproducible. It is aimed at having a krypton detection system which cannot be used only to analyze features of the distillation column but additionally as a diagnostic tool for different measurements in the course of the XENON100 and XENON1T experiments.

CHAPTER 2

Detection of trace concentrations of krypton in xenon

As it has already been discussed, to measure krypton in ppt concentrations new methods had to be developped. One possibility is to make use of the time delay of the two decay probabilities mentioned in chapter 1.3. There are further possibilities: on the one hand the atom trap trace analysis (ATTA), on the other hand the gas chromatrography mass spectrometry (GC-MS). In the ATTA setup, Krypton atoms are detected in an atom trap by their fluorescence light with a CCD camera or an avalanche photo diode [Che99]. However, this technique requires to cool down the krypton atom to the milli Kelvin range by laser cooling which is quite laborious. In the GC-MS setup, the krypton is separated from the gas sample, exploiting its physical and chemical properties (polarity, melting and boiling points and vapor pressure). The gas sample to be analyzed is carried through a column by an inert gas. The components of the gas react with the sides of the column causing a different elution time for each component. Then, a mass spectrometry can be used to detect the krypton that has been separated in the column [Gro04]. For this thesis, another setup is used, namely a residual gas analyzer (RGA) mass spectrometer enhanced by a cold trap. In this chapter the functioning of this method to detect very low concentrations of krypton in xenon is developped from a theoretical point of view.

2.1 Problems of the detection with a residual gas analyzer

RGA's have an upper pressure limit above which they cannot operate and are destroyed. This poses a problem for the detection of trace amounts of krypton in xenon. Typically, the pressure limit is about 10^{-5} Torr $\approx 1.332{\cdot}10^{-5}$ mbar [Dob11]. The total pressure is dominated by the xenon gas. If the RGA is sensitive down to partial pressures of 10^{-14} mbar, which is already very idealized, then only krypton concentrations in the order of magnitude of 10^{-9} mol/mol ($^{\mathrm{nat}}$Kr/Xe) can be measured (the partial pressure is proportional to the concentration at constant flow rate). Therefore, the RGA is at least three orders of magnitude too less sensitive to measure ppt concentrations of krypton.

The idea to enhance the measurable range of the RGA is to remove most of the xenon gas from the gas sample to not saturate the RGA. This is done by a cold trap (chapter 2.3).

2.2 Residual gas analyzer

The residual gas analyzer mass spectrometer consists of three main parts: the ionizer, the mass filter and the detector. In the following subsections they are explained in detail. For the setup, the RGA Transpector 2 H200 M is employed (chapter 3.1).

2.2.1 Ion source

The ionizer cage ionizes the incoming gas molecules by bombarding them with electrons. These electrons are created in a filament made of an iridium wire with thorium-oxide or yttrium-oxide which is heated by a DC current [Inf07]. Once the atoms of the gas sample are ionized, they can be manipulated by electric fields. The ions are accelerated towards a focus lens and formed into a beam. Some of these ions collide with the lens creating a current which is used to measure the pressure inside the ionizer to avoid destruction of the RGA by overpressure (figure 2.1). In ultra high vacuum normally single charged ions are predominant. But depending on the energy of the ionizing electrons, also multiple charged ions can be created.

$$\begin{gathered} \mathrm{A} + e^- \rightarrow \mathrm{A}^+ + 2e^- \\ \mathrm{A} + e^- \rightarrow \mathrm{A}^{2+} + 3e^- \\ \mathrm{A} + e^- \rightarrow \mathrm{A}^{3+} + 4e^- \end{gathered} \tag{2.1}$$

This information is of crucial importance for the analysis of the mass spectrum.

The ionization energy (IE) is the minimum amount of energy which has to be absorbed by an atom in the ground state to eject an electron. For the elements of interest in the gas phase, IE has the following values [Nis11]:

$$IE(\mathrm{Xe}) = 12.1\,\mathrm{eV} \tag{2.2}$$

$$IE(\mathrm{Kr}) = 14.0\,\mathrm{eV}. \tag{2.3}$$

If the ionizing electron only carries the ionization energy, the probability for the ionizing process to occur is very low because all of its energy would have to be transferred to the atom to ionize it. The cross section (which is defined as the area through which the electron must travel to interact with the atom) is close to zero. Almost independently on the atomic mass, the biggest cross section is reached when the kinetic energy of the electron is about 70 eV. However, the curve of the ionization probability versus electron energy is not equal for all elements[1] [Gro04]. In the Transpector 2 the electron energy is set at 102 eV [Inf07].

---

[1] This might cause a problem when analyzing the results quantitatively.

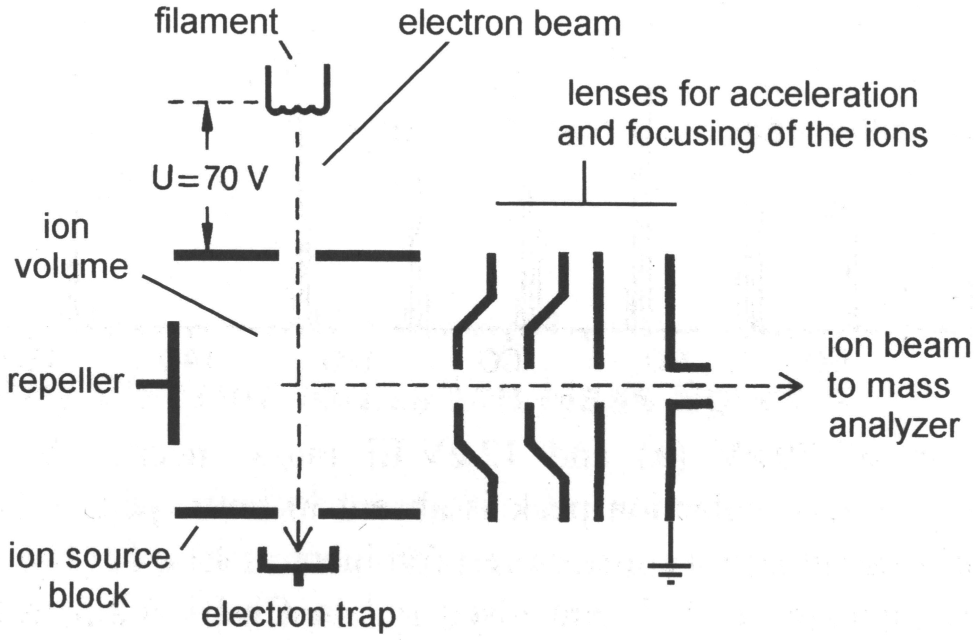

Figure 2.1: **Schematic sketch of the ionizer.** The ionizer consists of a heated filament which creates an electron beam. This is accelerated by a potential (in this case $U = 70$ V) and directed towards an electron trap. On their way, the electrons ionize the gas atoms in the ion volume. These ions are formed into a beam by several lenses. The last lens is grounded and called exit lense. One part of the beam, proportional to the pressure in the ion chamber, strikes this lense and creats a current which is measured to avoid overpressure [Gro04].

2.2.2 Quadrupole mass filter

The mass filter only lets through particles of a specific mass to charge ratio $\frac{m}{z}$. To discriminate the particles, it uses the static hyperbolic potential

$$\Phi(x, y) = \frac{\Phi_0}{2r_0^2}(x^2 - y^2) \tag{2.4}$$

along the z-axis. This potential can be created by four hyperbolic electrodes which have a rotational symmetry concerning the z-axis. Opposite electrodes are set on the potentials $+\Phi_0/2$ and $-\Phi_0/2$ respectively. Usually, the hyperbolic electrodes are approximated by cylindric ones for production reasons. The electrons are accelerated in the z-direction by an electric field. The electrodes then produce a force in x-direction,

$$F_x = q \cdot E_x = -q \cdot \nabla\Phi(x, y) = -\frac{qU}{r_0^2} \cdot x < 0, \tag{2.5}$$

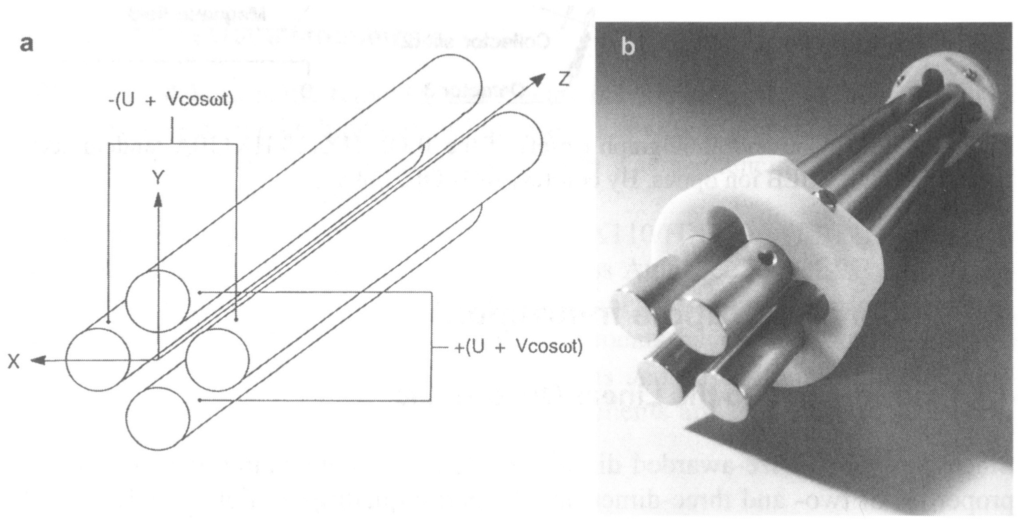

Figure 2.2: **The quadrupole mass filter.** On the left hand side the quadrupole mass filter is sketched schematically. Opposite rods are set on the same potential $\Phi(x, y)$, a DC voltage superimposed by an AC voltage. On the right hand side a photo of a mass filter is shown [Gro04].

and a second force in y-direction,

$$F_y = q \cdot E_y = +\frac{qU}{r_0^2} \cdot y > 0, \tag{2.6}$$

where $\Phi_0 = U$. Whereas the force in x-direction stabilizes the ion and produces harmonic oscillations, the force in y-direction makes the ion leave the y-axis exponentially and eventually it collides with the electrodes where the ion is neutralized.

In order to stabilize the trajectories in both directions, the DC voltage is superimposed by an AC voltage:

$$\Phi_0 = U + V\cos(\omega t). \tag{2.7}$$

So the electrons are stabilized during half a period in x-direction and destabilized in y-direction and vice versa in the following half of the period. The equations of motion are

$$\ddot{x} + \frac{q}{mr_0^2}(U + V\cos\omega t)x = 0 \tag{2.8}$$

$$\ddot{y} + \frac{q}{mr_0^2}(U + V\cos\omega t)y = 0. \tag{2.9}$$

With the abbreviations

$$a = \frac{4qU}{mr_0^2\omega^2},\ b = \frac{2qV}{mr_0^2\omega^2},\ \tau = \frac{1}{2}\omega t \tag{2.10}$$

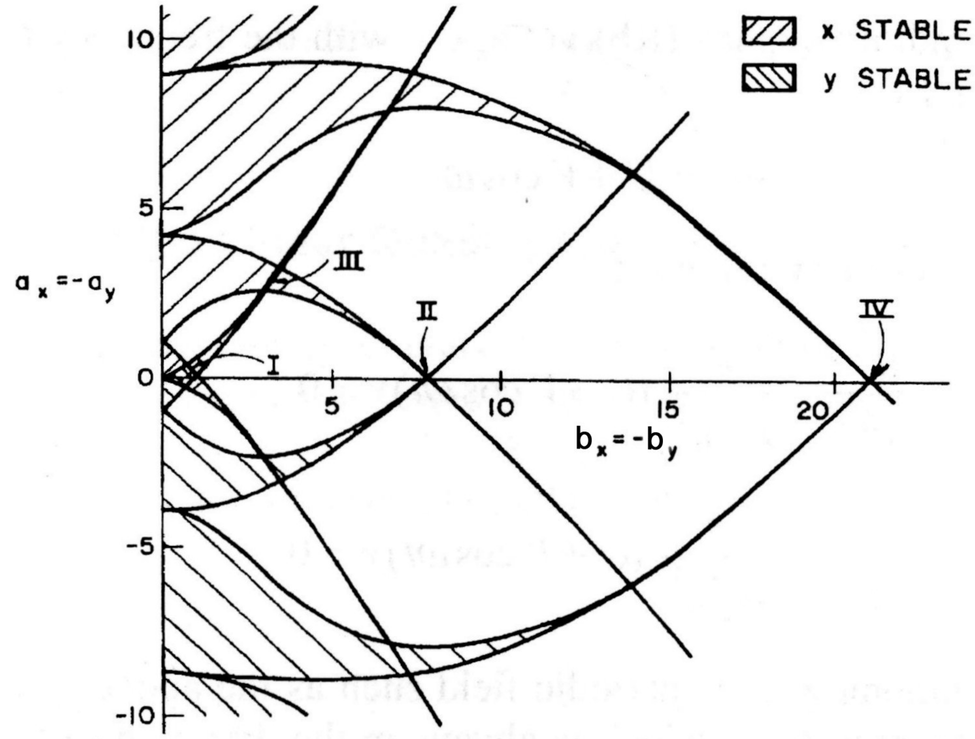

Figure 2.3: **Stability diagram of a quadrupole mass filter.** In the stability diagram, stable regions for the x- and y-direction are marked for the parameters a and b. There are four main stable regions where the movement is stable both in x- and y-direction (labeled with I-IV). Typically, region I is considered since it is the largest one [Gro04] (modified).

these equation can be formulated as

$$\frac{\mathrm{d}^2x}{\mathrm{d}\tau^2} + (a + 2b\cos 2\tau)x = 0, \quad (2.11)$$

$$\frac{\mathrm{d}^2y}{\mathrm{d}\tau^2} + (a + 2b\cos 2\tau)z = 0. \quad (2.12)$$

This type of equation is called Mathieus's differential equation. Depending on the values of a and b, the solution is

- **stable**, that means that the ions oscillate with a limited amplitude throughout the length of the quadrupole, or
- **unstable**, that means that the amplitude of the oscillations increase and the ions collide with the electrods before reaching the end of the quadrupole.

.

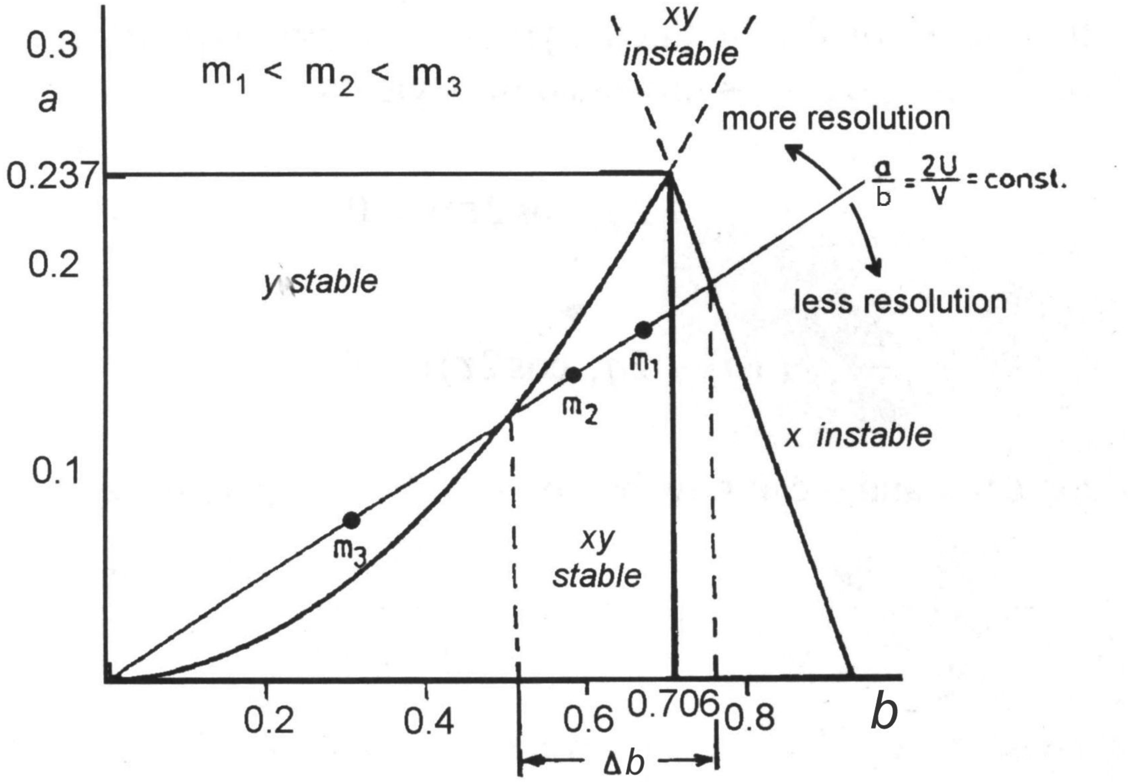

Figure 2.4: **Detail of the stability diagram of a quadrupole mass filter.** This diagram provides a closer look at the stability region I of figure 2.3. The load line is determined by the ratio $2U/V$. The difference Δb defines the sensitivity of the mass filter. $1/b$ is proportional to the mass to charge ratio m/z. That is why $m_2 > m_1$ for the same charge $z = 1$ [Gro04] (modified).

The stable areas are illustrated in an a-b-diagram (figure 2.3). The ratio

$$\frac{a}{b} = 2 \cdot \frac{U}{V} = \text{const.} \tag{2.13}$$

only depends on the values of U and V. This ratio defines a load line. For some mass to charge ratios m/z, this load line crosses the stable areas in the a-b-diagram. Therefore, by changing the voltage parameters, the interval of stable mass to charge ratios can be determined [Dem10].

2.2.3 Ion detector

The ions which do not collide with the rods are analyzed in the detector. This analyzing section can contain a Faraday cup (FC) or an Electron multiplier (EM) or both.

- **Faraday cup:**
  The Faraday cup simply consists of a metal plate which is at ground potential.

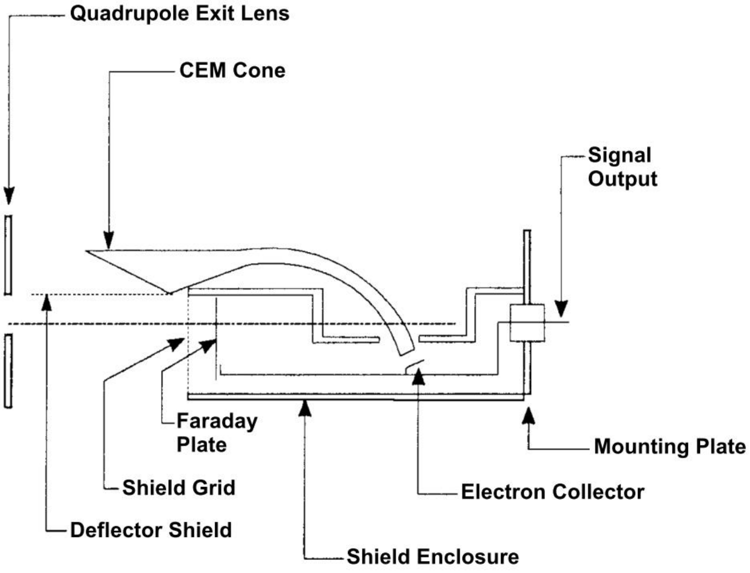

Figure 2.5: **The channel electron multiplier (CEM)/Faraday cup detector.** This detector combines the electron multiplier with a Faraday cup. If negative voltage is applied to the deflector shield, incoming positive ions are directed towards the CEM cone where the ions remove secondary electrons by collision (electron multiplier). These electrons reach the electron collector which creates the signal. If the deflector shield is at ground potential, the electrons collide with the Faraday plate resulting in a smaller current which, however, is precise enough to do quantitative measurements [Inf07].

Incoming ions are neutralized by the electrons in the plate resulting in a current which is equal to the incoming ion current. Therefore, the Faraday cup is a very precise instrument for quantitative measurements [Inf07].

- **Electron multiplier:**
  When entering the electron multiplier, the ions are accelerated by a high negative voltage ($U \approx -1$ kV). Once they strike the multiplier surface, secondary electrons are emitted. These electrons are itself accelerated and once again liberate electrons of another surface. This process is repeated various times. At the end, the electrons are collected by a Faraday cup. One ion therefore creates a million electrons or so. This is why EM are highly sensitive and allow to measure partial pressures of $p_{\text{part}} = 2.7 \cdot 10^{-14}$ mbar whereas the FC is only sensitive up to $p_{\text{part}} \approx 10^{-12}$. A disadvantage of the EM is that the ratio of created electrons for an incoming ion is not stable. Thus it is less appropriated for quantitative measurements [Inf07].

There are also combinations of a Faraday cup and an electron multiplier (figure 2.5).

2.3 Cold trap

The cold trap is used to remove most of the xenon from the gas sample in order to not saturate the RGA. It consists of an U-bend which is cooled down to $T = 77.3$ K by liquid nitrogen.

The cold trap exploits the phenomenon of vapor pressure, more precisely of sublimation vapor pressure. At low melting temperatures, the gas phase and the solid phase can coexist (at the temperature of liquid nitrogen, xenon has no liquid phase). The pressure at which these two states are in equilibrium is called (sublimation) vapor pressure.

The reason for this coexistence is the following: The energy of particles in a solid is distributed following the law of the Maxwell Boltzmann distribution

$$F(E) \propto \exp(-\frac{E}{kt}) \tag{2.14}$$

$$E = \frac{1}{2}mv^2. \tag{2.15}$$

That is why there is always a fraction of particles whose energy exceeds the energy that is needed to leave the solid. These particles are responsible for the vapor pressure. The dependence of vapor pressure on the temperature can be calculated using the Clapeyron relation

$$\frac{\mathrm{d}p}{\mathrm{d}T} \approx \frac{\Delta s_m}{\Delta v_m} \tag{2.16}$$

where Δs_m is the difference of the molar entropy and Δv_m the difference of the molar volume during the phase transition. For sublimation processes, this equation can be specified to

$$\frac{\mathrm{d}p}{\mathrm{d}T} = \frac{p \cdot \Delta q_s(T)}{k \cdot T^2} \tag{2.17}$$

where $\Delta q_s(T)$ is the sublimation enthalpy, that is the energy needed to sublimate a particle of the element in question [Rei10]. The sublimation enthalpy is the sum of the enthalpy of fusion and of vaporization. The differential equation can be solved resulting in a sublimation vapor pressure curve of

$$p_{\text{vapor}} = p_{\text{vapor},0} \cdot \exp\big[-\frac{\Delta q_s}{k_B}(\frac{1}{T} - \frac{1}{T_0})\big] \tag{2.18}$$

with an initial value $(p_{\text{vapor},0}, t_{\text{vapor},0})$. The values of vapor pressure for xenon and krypton for different temperatures are shown in figure 2.6. The formula derived above can be used to calculate this value using an already measured value pair as initial point. With $(p_{\text{vapor},0}, t_{\text{vapor},0}) = (267\,\text{mbar}, 148\,\text{K})$ as a starting point and $\Delta q_s = 14.94$ kJ/mol, one gets

$$p_{\text{vapor}}^{\text{T(LN}_2\text{)}} \approx 4 \cdot 10^{-3}\,\text{mbar}. \tag{2.19}$$

Table 2.1: **Melting and boiling points and vapor pressure** at the temperature of liquid nitrogen for krypton and xenon [Pol64] [Gru64].

Gas	T_{boil}(K)	T_{melt}(K)	$p_{\text{vapor}}^{\text{T(LN}_2)}$(mbar)
Kr	119.9	115.8	≈ 2
Xe	165.0	161.4	$2.4{\cdot}10^{-3}$

This simple estimation does not provide a very exact value, however the order of magnitude is correct. The exact value for xenon was measured to be

$$p_{\text{vapor}}^{\text{T(LN}_2)} \approx 2.4 \cdot 10^{-3}\,\text{mbar} \quad \text{[Gru64]}. \tag{2.20}$$

For the temperature of liquid nitrogen, vapor pressures are listed in table 2.1 together with the melting and boiling points at atmospheric pressure.

While the xenon gas flows through the cold trap, it cools down to $T = 77.3$ K and freezes to the wall. Independently from the incoming partial pressure of xenon (which is almost equal to the total pressure of the sample since the fraction of impurities is in the order of 10^{-6}), the outcoming pressure should be equal to the vapor pressure $p_{\text{vapor}}^{\text{T(LN}_2)} = 2.4 \cdot 10^{-3}$ mbar. The krypton instead remains unaffected. Although the krypton also has a melting temperature above that of liquid nitrogen, it does not freeze because at 77.3 K its partial pressure is far below the solid-vapor or liquid-vapor equilibrium. That is why the impurities pass the cold trap.

The vapor pressure of xenon is still too high for the RGA. To avoid its saturation, the gas is pumped through a differential low conducting pumping section (DPS, 3.4) where the pressure is reduced to $\lesssim 10^{-5}$ mbar.

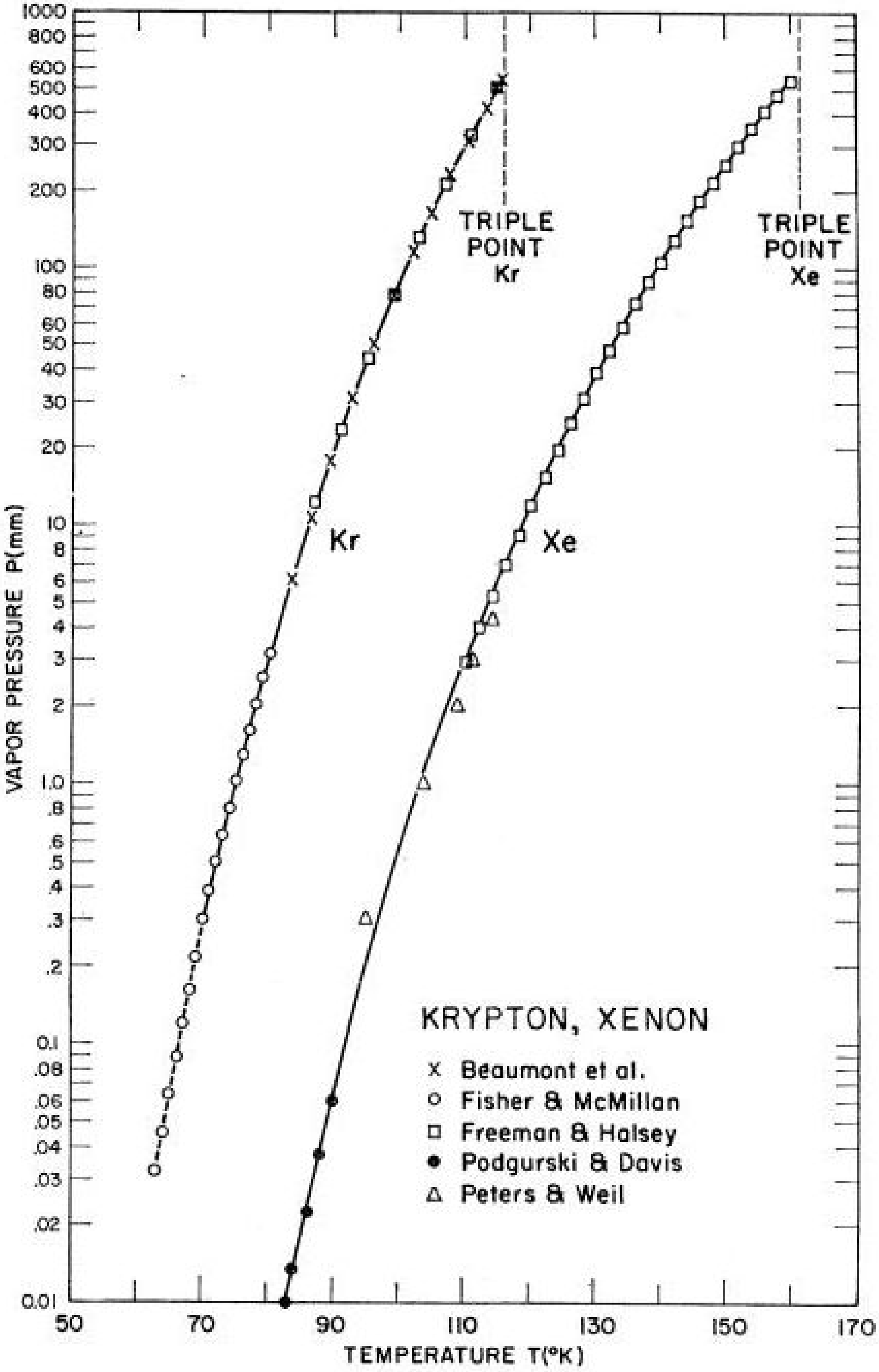

Figure 2.6: **Vapor pressure of xenon and krypton at different temperatures** [Pol64].

CHAPTER 3

Experimental setup

By now, it has become evident why krypton detection at very low levels is essential for the XENON1T experiment (chapter 1.3) and how detection by a RGA enhanced by a cold trap—in principle—works (chapter 2). In this chapter, the experimental setup will be explained in detail. At first it is sketched schematically and then compared to a test setup that has been built for a diploma thesis in Münster. Subsequently, the different parts of the setup are explained in detail. The installation of the setup and the experiments were done under the supervision of Ph.D. student Stephan Rosendahl.

3.1 Setup in the XENON laboratory

In the context of this bachelor thesis, the mass spectrometer enhanced by a cold trap was installed at the main setup in the XENON laboratory in Münster. Later, this setup will be completed by a test distillation column which can then be calibrated by this krypton detection system.

The core of the setup is the residual gas analyzer Inficon Transpector2 H200 M whose functioning has been described previously (chapter 2.2). The detector uses both a Faraday cup and an Electron multiplier combined in one unit [Inf07]. However, if one wishes to use only one of the instruments, the other can be turned off.

Different pressure gauges are used: p_9 and p_{10} are measured by Oerlikon Penningvac PTR 90 pressure gauges which are gas dependent. For pressures below $p = 10^{-5}$ mbar, there is a conversion factor $k_{\mathrm{Xe}} = 0.4$ for xenon to calculate p_{eff}. On the contrary, p_8 is measured by a MKS Baratron 121 A which directly measures the force per unit area and therefore is gas independent.

VCR fittings of the company Swagelok made of stainless steel are used for the gas system. Orbital welding has been employed to guarantee leak-tightness.

The main components of the setup are shown in figure 3.1.

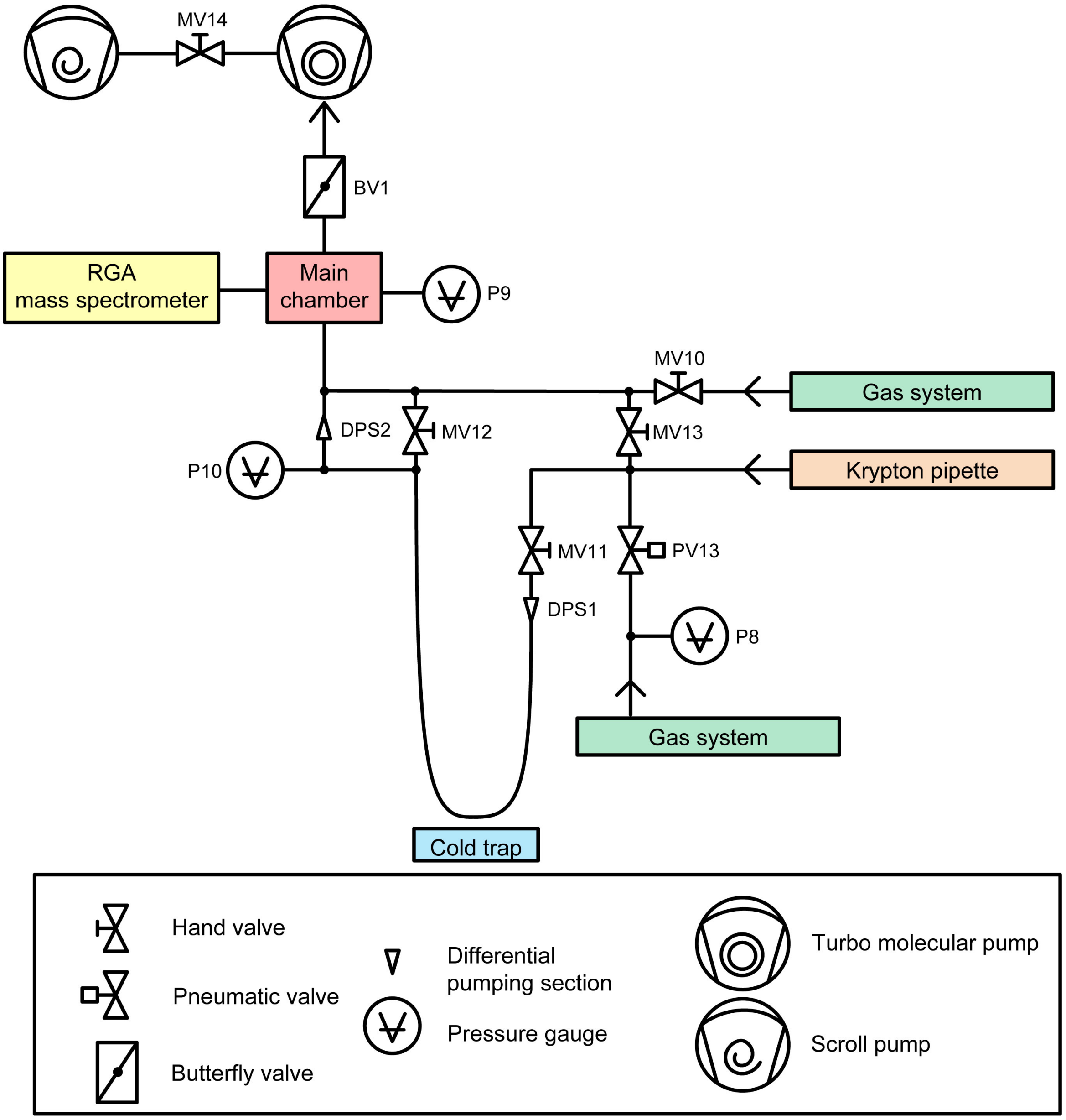

Figure 3.1: **Schematic sketch of the setup.** The sample gas is introduced via the pneumatic valve PV13. MV10, MV12 and MV13 remain closed while MV11 is open. The differential pumping section DPS1 behind MV11 reduces the gas pressure before the gas enters the cold trap where the xenon freezes. Behind the cold trap, pressure is further reduced by DPS2 before entering the main chamber. The butterfly valve allows to manipulate the pumping speed of the turbo molecular pump. Thus the sample gas remains for a longer time in the main chamber where it is analyzed by the RGA. MV12 and MV13 are only opened to evacuate the system.

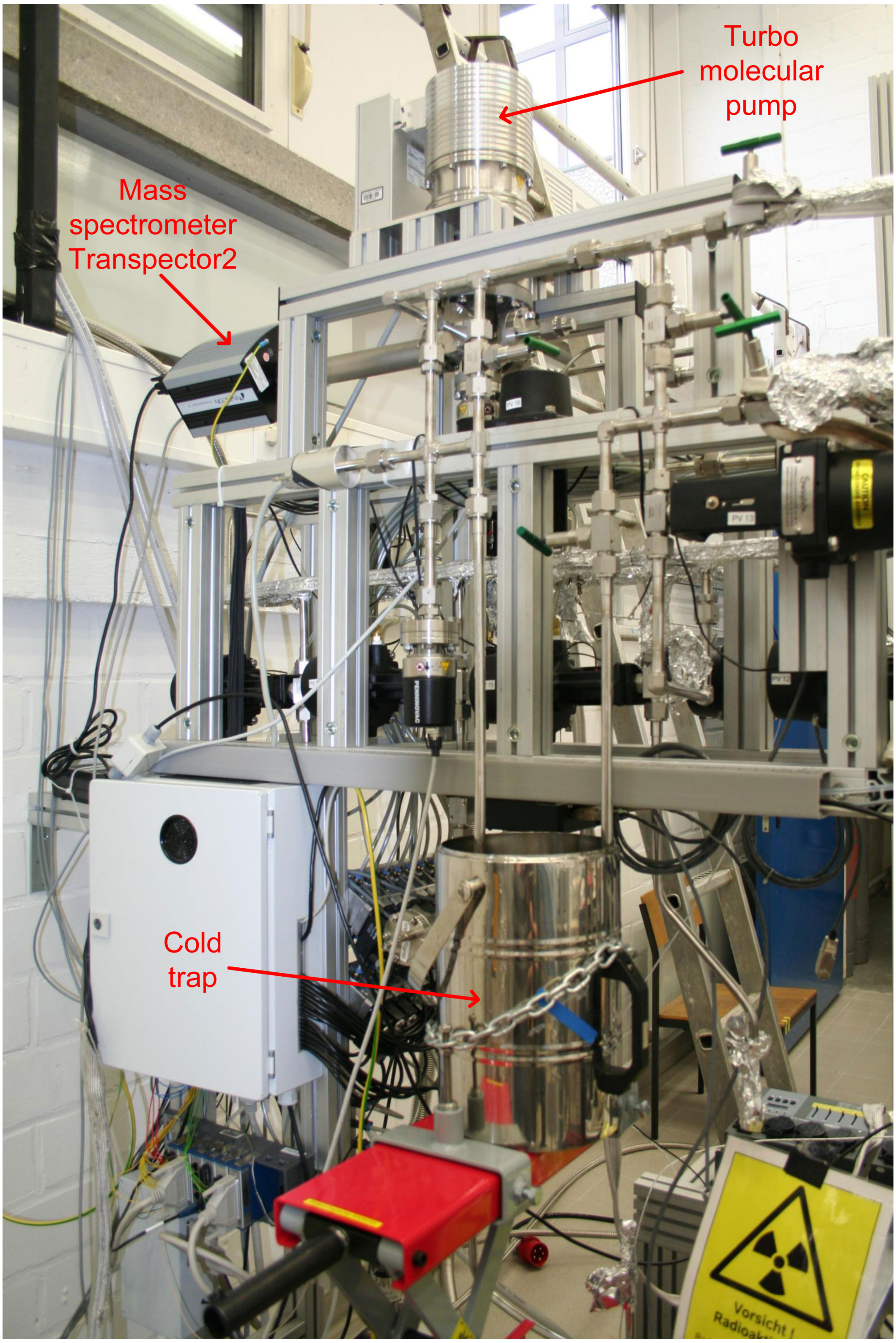

Figure 3.2: **Photo of the setup.** In the foreground, there is the cold trap vessel filled with liquid nitrogen on a lifting platform which is manipulated by hand. The mass spectrometer and the turbo molecular pump are situated at the top of the system. The scroll pump (not in the picture) operates at the bottom.

3.2 Comparison with the test setup

In the context of a diploma thesis, the mass spectrometer enhanced by a cold trap had been installed on a test setup beforehand in order to see if this technique is—in principle—appropriate for the detection of trace concentrations of krypton in xenon [Ket12]. The tests have been successful. At first, the limit for the sensitivity of krypton detection was measured to be (6.5 ± 1.5) ppb Kr/Xe, thus being three orders of magnitude too less sensitive for the calibration of the distillation column.

An enhancement was reached by reducing the effective pumping speed of the turbo molecular pump. The reason for this is the fact that most of the gas sample in the main chamber is removed by the turbo molecular pumping system before being ionized. Therefore, the ionization efficiency for an atom in the ionizing region is small, due to the large mean free pathes of both the electron and the atoms. By reducing the pumping speed of the turbo molecular pump, the sensitivity of the test setup could eventually be enlarged to ≈ 100 ppt Kr/Xe.

Technically, the reduction of effective pumping speed was done simply by partially closing a VAT UHV gate valve which separated the main chamber with the RGA from the turbo molecular pump. It was "moved 14.5 turns until the gate [was] close to catch" [Ket12]. It is evident that this technique is hardly reproducible and cannot be analyzed quantitatively in an appropriate manner. That is why a butterfly valve has been installed between the main chamber with the RGA and the turbo molecular pump (chapter 4.3). It allows gradual changes of the flow rate between the two components.

3.3 Vacuum conditions in the setup

The quality of the vacuum sets a limit to the sensitivity of the system. The experimental setup for this thesis requires an ultra high vacuum which is normally considered to be in the range of $p = 10^{-7} - 10^{-12}$ mbar. First pressure is reduced by an oil-free scroll pump (Scroll Vac SC 15D) to $p \approx 10^{-2}$ mbar. When this pre-vacuum is established, a turbo molecular pump (Leybold Turbo Vac MAG W 300 P) is used to further reduce the pressure. By this method, a vacuum of $p \approx 5 \cdot 10^{-9}$ mbar is reached.

To reach such a vacuum, all parts have to be ultra clean. Therefore, before assembling the components, they have been cleaned in an ultra-sonic bath. The connection surfaces additionally have been cleaned with ethanol.

After the setup had been completed, the system was baked out at 80 °C (the part with the mass spectrometer) and 130 °C (the rest) in order to reduce contamination with water molecules, hydro-carbon molecules and other impurities.

3.4 Differential low conduction pumping section

One of the main motivations of this thesis was the construction of an user-friendly diagnostic tool for the krypton detection in xenon which can be used with gas input pressures up to $p \approx 2$ bar without requiring much manipulation by the experimenter. To reduce pressure, two differential low conduction pumping sections are needed.

The first capillary DPS1 has a diameter of $d = 0.13$ mm and a length of $l = 100$ mm. It reduces the inlet pressure before the gas enters the cold trap to make sure that all the xenon gets frozen.

The second capillary DPS2 has a diameter of $d = 1$ mm and a length of $l = 5$ mm. It is required to reduce the pressure in order to not saturate the RGA. The saturation pressure is $p_{\text{sat}} \approx 6.7 \cdot 10^{-4}$ mbar [Inf07]. The outcoming pressure of the cold trap is about $p_{\text{vapor}}^{\text{T(LN}_2)} = 2.4 \cdot 10^{-3}$ mbar. Thus pressure has to be reduced behind the cold trap by about two orders of magnitude to allow also the employment of the butterfly valve. This is done by a differential low conduction pumping section (DPS).

Technically, the DPS segment is laser-welded into a VCR gasket (figures 3.3, 3.4) which turned out to be the best design for an effective pressure reduction. The capillaries were produced by the mechanical workshop of the Institut für Kernphysik in Münster.

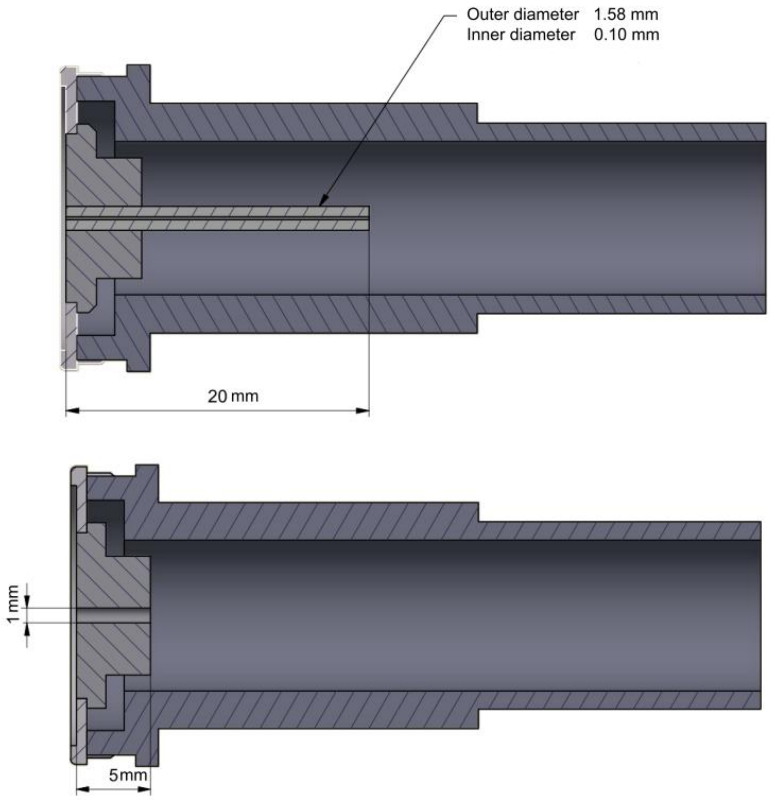

Figure 3.3: **Technical drawing of the differential pumping section.** This drawing shows capillary DPS1 at gas inlet (above) and DPS2 behind the cold trap and its dimensions. In the final setup, the length of DPS1 has been changed to 100 mm.

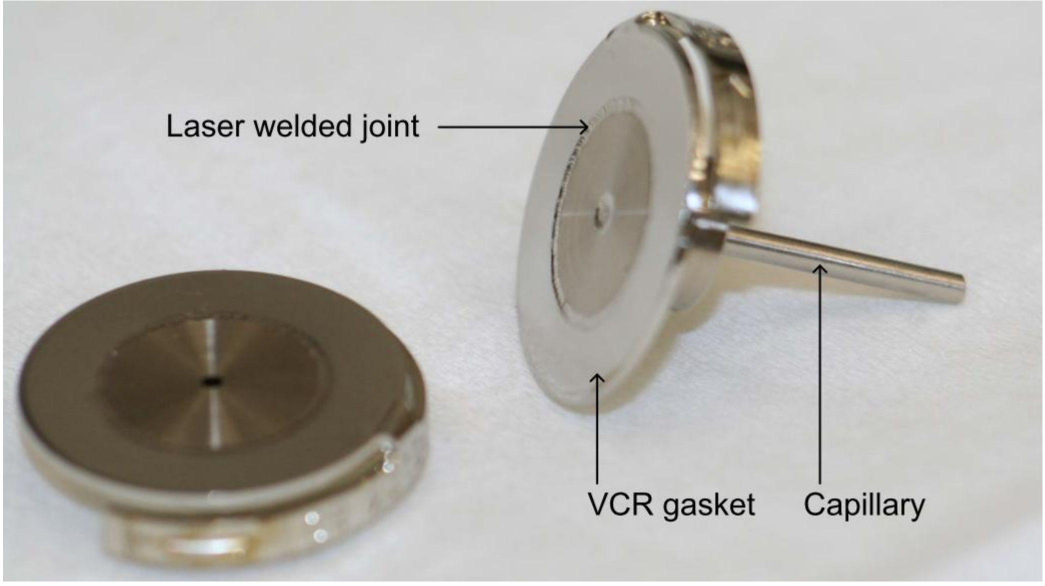

Figure 3.4: **Photo of the differential pumping section.** The capillary is welded into a VCR gasket.

3.5 Butterfly valve

Butterfly valves are used to regulate the flow in fluid systems. In this setup, they are used to reduce the flow rate between the main chamber with the RGA and the turbo molecular pump. A disc of a diameter of $d = 54.6$ mm and thickness of $b = 1$ mm is used as a closing mechanism. The thickness is very small compared to the diameter and can therefore be neglected. The disc can be turned gradually by hand by turning a rotary feedthrough which has a scale on it with steps of one degree (figure 3.5). The value can be fixed with a screw.

The valve itself consists of a distance flange CF-100 with a hole in the center (diameter $d = 55$ mm) where the disc is placed. For the rotary feedthrough a CF-16 sideport is added. The distance flange is mounted to the turbo molecular pump on the one side and to the main chamber with the RGA on the other side via a M8 threaded rod. The sealing ring is made of copper.

The usage of this butterfly valve is more convenient compared to the VAT valve used in the test setup, since the pumping speed of the turbo molecular pump can be manipulated in well defined steps of one degree and therefore in a reproducible way.

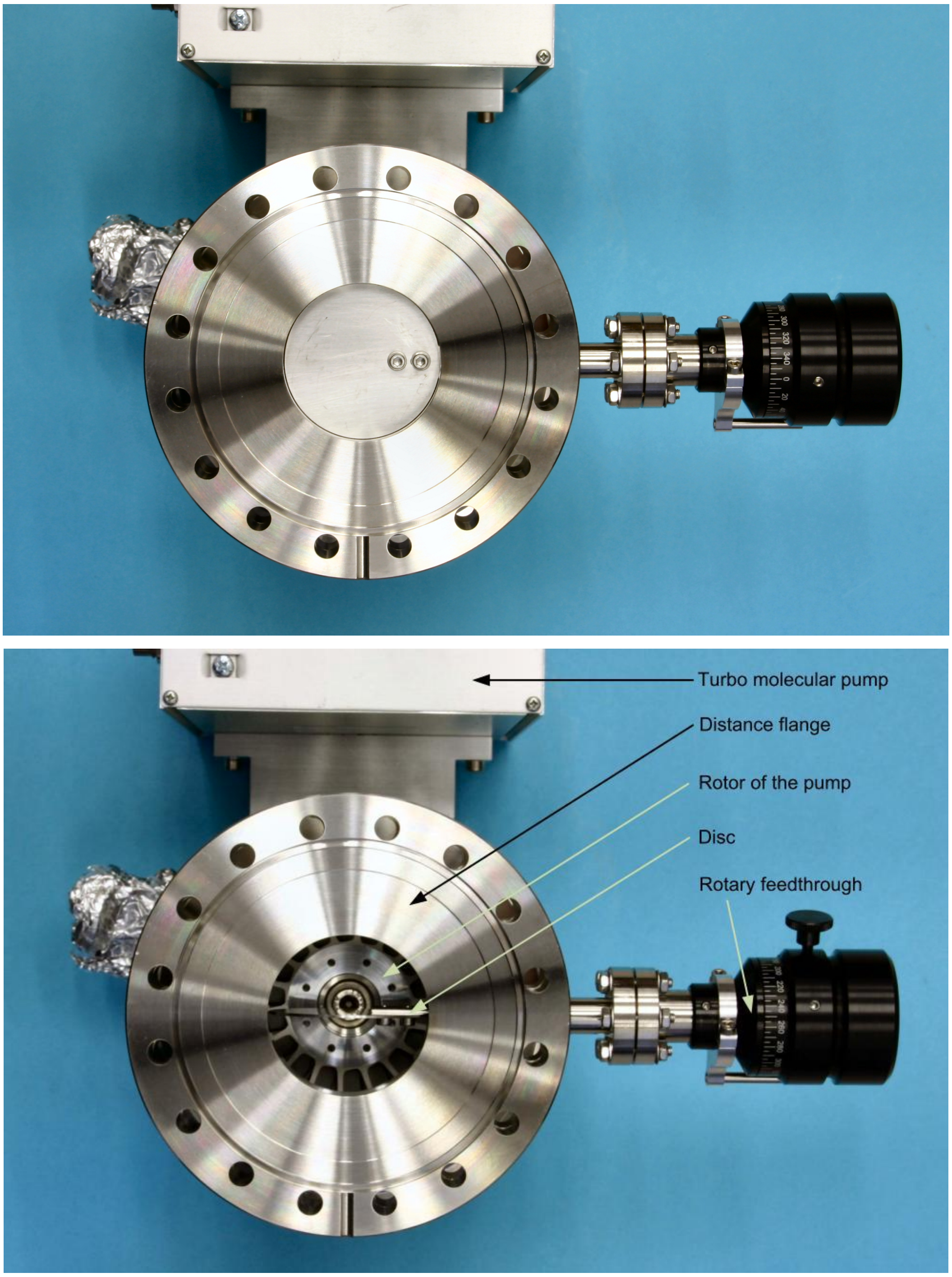

Figure 3.5: **The butterfly valve.** These photos show the butterfly valve provisionally mounted on the turbo molecular pump with the disc closed (above) and open.

CHAPTER 4

Gas flow in the system

With the RGA/cold trap setup, it is aimed at having an analysis tool for different applications. In this chapter the gas flow in the system is examined to theoretically understand the setup.

One of the major tasks of this bachelor project was the construction of a krypton detection system which is easy to handle and only needs a minimum of adjustments when used as a diagnostic tool for different applications in the XENON experiments. This requires pressure reduction in different steps (chapter 4.2, 4.3) which are now examined in detail.

When one wants to describe such a fluid system quantitatively, one has to calculate the (fluid) conductances of the different segments, that is the ability for fluids to pass the segment[1]. Conductances can be calculated in two different manners. They can be theoretically derived using the the geometric dimensions of the segment and calculated measuring the pressure drops in front of and behind the segment. In the following sections, the theoretical and the experimental values for the differential pumping section and the butterfly valve are calculated and compared.

4.1 Flow types

When calculating conductances, it is necessary to know the flow type in the segment in question. The flow types are distinguished by the Knudsen number

$$Kn = \frac{\bar{l}}{d} \tag{4.1}$$

where $\bar{l}$ is the mean free path of the gas molecules and d the diameter of the pipe [Jou06]. There are three different flow types.

---

[1] Analysis of fluid systems are done in a theoretical frame analogous to that of electric systems. The fluid conductance is comparable to the electric conductance which is the inverse of the resistance.

- **Molecular flow:**

  $$Kn > 0.5 \tag{4.2}$$

  The mean free path is long compared to the diameter of the pipe. Particles almost do not collide with each other.

- **Knudsen flow:**

  $$0.5 > Kn > 0.01 \tag{4.3}$$

  The Knudsen flow is a transition regime between the molecular flow and the viscous flow. The particle collide with each other approximately as often as they collide with the pipe walls.

- **Viscous flow:**

  $$Kn < 0.01 \tag{4.4}$$

  In viscous flow, particles constantely collide with each other, thereby exchanging energy and momentum.

When considering a pipe which is long compared to its diameter, the viscous flow is further subdivided in laminar and turbulent flow. In a long pipe with a circular cross section the gas molecules near the sides of the pipe are slowed down due to friction effects. However if the velocity is relatively low, all the volume elements in the pipe go in the same direction, those near to the sides of the pipe slower than the others (laminar flow). But if the velocity increases, the faster volume elements in the centre of the pipe are distracted towards the sides. This effect causes turbulence having impact on the conductivity (turbulent flow) [Jou06]. In this region, higher poressure does not result in a significantly higher flow rate anymore. For a relatively long pipe with a circular cross section the condition to decide whether laminar or turbulent flow is given is

$$\begin{aligned} Re & \begin{cases} < 2300 & \text{laminar flow} \\ > 4000 & \text{turbulent flow} \end{cases} && (4.5) \\ Re &= \frac{32}{\pi^2} \cdot \frac{q_{\mathrm{pV}}}{\eta \cdot \overline{c}^2 \cdot d}, && (4.6) \end{aligned}$$

where η is the viscosity of the gas and d the diameter of the pipe, $\overline{c}$ is the average speed of the gas molecules, q_{pV} the flow rate through the segment [Jou06].

4.2 Conductances of the differential low conducting pumping sections

4.2.1 Differential pumping section 1

DPS1 reduces the pressure of the gas entering the cold trap. The incoming pressure is about $p_8 \approx 1-2$ bar. It can therefore be assumed that we are in the region of viscous flow. To determine whether the flow is laminar or turbulent, the Reynold number *Re* becomes relevant. The flow through the segment is given by q_{pV} which has to be determined by measurements, analyzed below. q_{pV} is dependent on the inlet gas pressure. In figure 4.1, *Re* is plotted versus the inlet pressure p_8 for

$$\eta_{\text{Xe}}^{T=293.15\,\text{K}} = 2.3 \cdot 10^{-5}\,\frac{\text{kg}}{\text{ms}} \quad \text{[Jou06]}, \tag{4.7}$$

$$\bar{c} = \sqrt{\frac{8 \cdot R \cdot T}{\pi M}} = 217.426\,\frac{\text{m}}{\text{s}}. \tag{4.8}$$

From the figure one concludes that throughout the whole pressure range laminar flow can be supposed.

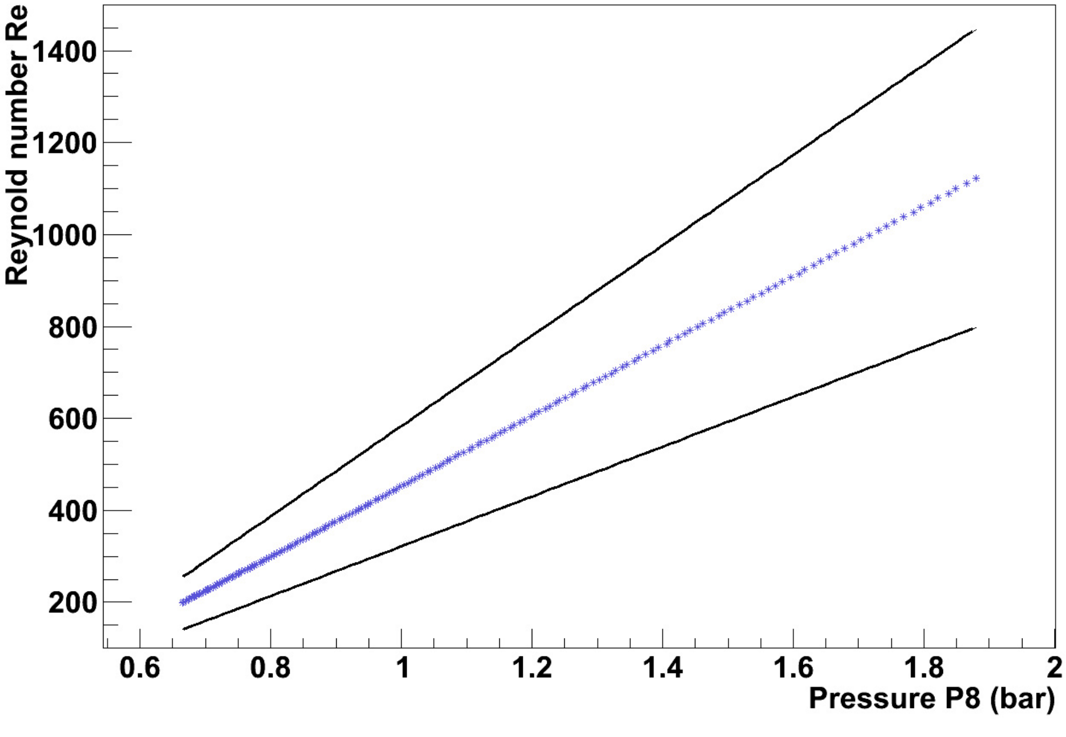

Figure 4.1: **Reynold number of DPS1 for different inlet pressure.** The Reynold number for an inlet pressure up to 2 bar remains below $Re = 2300$. Therefore, laminar flow can be assumed. The limits of the error region are marked by the black lines. The error is unusually large due to the error of a volume element which could only be determined in a margin of ±30 % (see below).

- **Geometrical conductance:**
  The conductance for a tube of circular cross section—laminar flow supposed—is

$$C_{\mathrm{DPS1}}(p_8) \approx \frac{\pi}{256} \cdot \frac{1}{\eta} \cdot \frac{d^4}{l} \cdot p_8, \tag{4.9}$$

$$[C_{\mathrm{DPS1}}] = \frac{\mathrm{L}}{\mathrm{s}} \tag{4.10}$$

  where $\eta_{\mathrm{Xe}}^{T=293.15\,\mathrm{K}} = 2.3 \cdot 10^{-5}$ kg/(ms). As $p_{10} \ll p_8$, it can be ignored. Therefore, the value is valid independently from whether the cold trap is cooled down or not.

- **Measurement of the conductance:**
  If the pressure drops, the volume in front of the DPS and the pressure-time characteristic is known, the conductance can be calculated. The flow through DPS1 is determined by the volume V in front of the capillary. V has been estimated to $V = (0.17 \pm 0.05)$ L. A conservative error of 30 % has been chosen.

$$q_{\mathrm{DPS1}} = V \cdot \frac{\mathrm{d}p_8}{\mathrm{d}t} \tag{4.11}$$

  On the other hand q_{DPS1} is determined by the conductance:

$$q_{\mathrm{DPS1}} = C \cdot (p_8 - p_{10}). \tag{4.12}$$

  With these equations one can derive that

$$C(p_8) = \frac{V \cdot \dot{p_8}}{p_8 - p_{10}}. \tag{4.13}$$

In the following figures 4.2 and 4.3 the values of both methods are compared for two different runs at different inlet pressures.

The error is dominated by the constant systematic volume error. The volume could only be determined within a margen of ±30 %. This error is very likely responsible for the y-offset of the measured conductance. As it can be seen in figure 4.2, if the volume error is taken into account, the geometrical and the experimental value are in good agreement.

Another property of the experimental conductance is the slope becoming smaller for high inlet pressure. This is probably an evidence for the fact that one is close to the transition from laminar flow to turbulent flow. Following the analysis of the Reynold number above, the turbulent flow regime is not yet reached for an inlet pressure of ≈ 2 bar. However the transition is gradual and therefore already has an impact on pressures $\lesssim 2$ bar. The increasing slope for little inlet pressures has not yet been theoretically understood.

The determination of this conductance is helpful to estimate the efficiency of the cold trap. For instance an inlet pressure of $p_8 = 1.88$ bar is reduced by DPS1 to $p = 0.77$ mbar (before entering the cold trap). The cold trap further reduces the pressure of the xenon gas to $p_{\mathrm{vapor}}^{\mathrm{T(LN_2)}} \approx 2.4 \cdot 10^{-3}$ mbar, thus by about two order of magnitudes. As krypton passes the cold trap unaffected, its concentration in the xenon is enhanced by the cold trap by about two orders of magnitude.

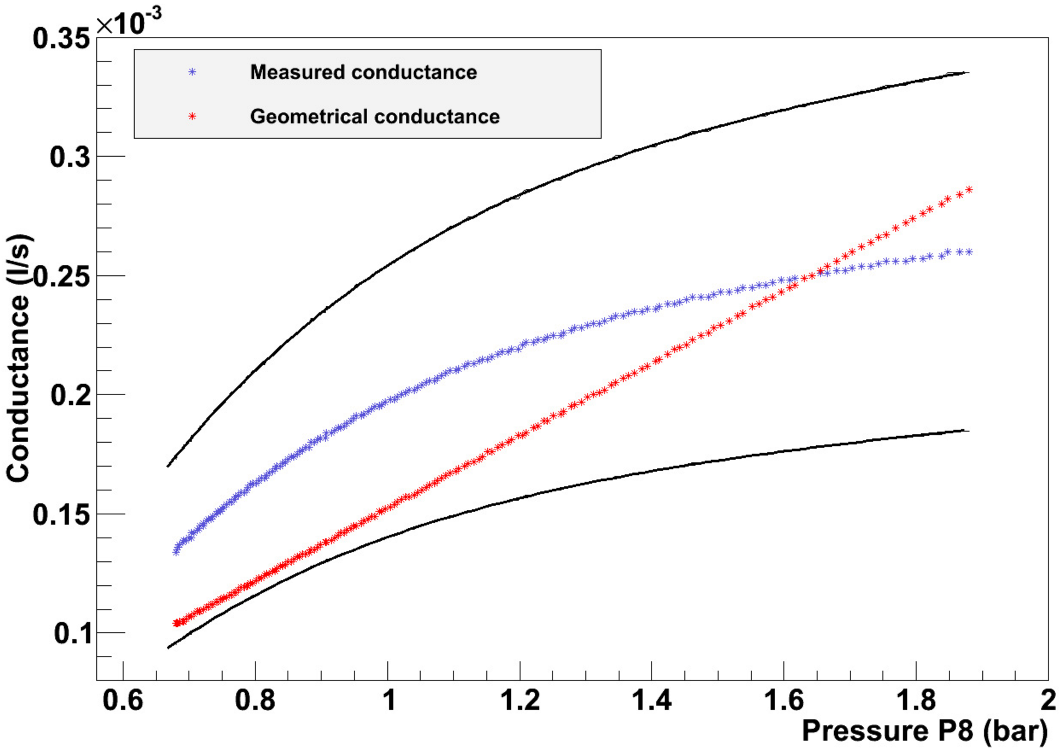

Figure 4.2: **Conductance of differential low conduction pumping section 1.** Run 1. The black lines mark the limits of the error of the measured value.

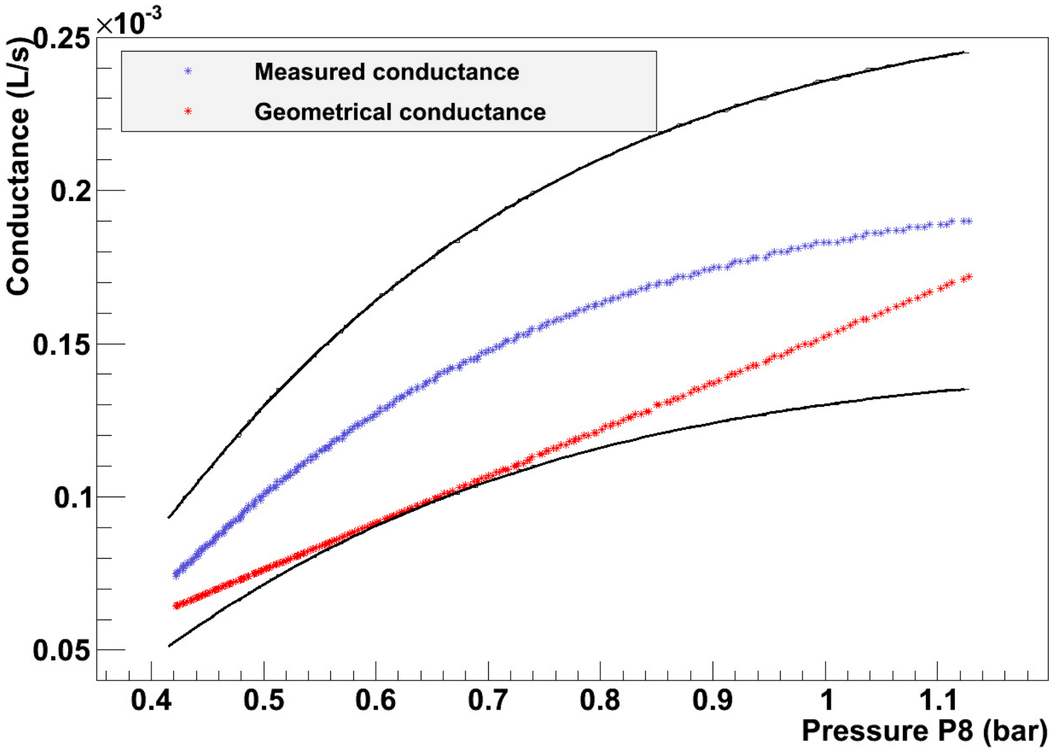

Figure 4.3: **Conductance of differential low conduction pumping section 1.** Run 2. The black lines mark the limits of the error of the measured value.

4.2.2 Differential pumping section 2

First, the flow type is investigated. Therefore, one has to calculate the Knudsen number:

$$Kn = \frac{\bar{l}}{d} = \frac{k_B T}{\sqrt{2} \cdot p_{10} \cdot d_{\mathrm{mol}}^2 d_{\mathrm{pipe}}} \approx 1.68 \geq 0.5. \tag{4.14}$$

That means that molecular flow is given. It has been assumed that $p_{10} = p_{\mathrm{vapor}}^{\mathrm{T(LN_2)}} = 2.4 \cdot 10^{-3}$ mbar; d_{mol} is two times the van der Waals radius $r_{\text{van der Waals}}^{\mathrm{Xe}} = 216$ pm [Bon64].

- **Geometrical conductance:**
  At the temperature of liquid nitrogen ($T = 77.3$ K) and for molecular flow, the conductance for the capillary is

$$C(\mathrm{Xe}) = \frac{\pi}{16} \cdot \sqrt{\frac{8 \cdot R \cdot T}{\pi M}} \cdot d^2 \frac{14 + 4\frac{l}{d}}{14 + 18\frac{l}{d} + 3(\frac{l}{d})^2} \tag{4.15}$$

$$= 4.11 \cdot 10^{-2}\, \frac{\mathrm{L}}{\mathrm{s}}. \tag{4.16}$$

- **Measurement of conductance:**
  If the pressure drops and the pumping speed are known, the conductance can be calculated. The effective pumping speed S_{eff} in the main chamber is, given that the butterfly valve is totally open (cf. chapter 4.3, the theoretical value is assumed),

$$S_{\mathrm{eff}} = \frac{C_{\mathrm{bf}} \cdot S}{C_{\mathrm{bf}} + S} \tag{4.17}$$

$$= 90.28\, \frac{\mathrm{L}}{\mathrm{s}}. \tag{4.18}$$

The effective pumping speed determines the flow through DPS2.

$$q_{\mathrm{DPS2}} = S_{\mathrm{eff}} \cdot p_9. \tag{4.19}$$

On the other hand is

$$q_{\mathrm{DPS2}} = C_{\mathrm{DPS2}} \cdot (p_{10} - p_9). \tag{4.20}$$

When vapor pressure has been reached in the cold trap, p_9 and p_{10} remain constant over time (equilibrium state):

$$p_{9,\mathrm{eff}} = 9.2 \cdot 10^{-7}\, \mathrm{mbar}. \tag{4.21}$$

The pressure $p_{10} = 3.9 \cdot 10^{-3}$ mbar displayed by the pressure gauge is not in a region where the gas dependent value can be transformed in the effective pressure value simply by a conversion factor. But as the value remains constant over a long period of time when the gas inlet is closed (more than 30 minutes), it is assumed that vapor pressure in the cold trap has been reached and the value is set to

$$p_{10} = 2.4 \cdot 10^{-3}\,\mathrm{mbar}. \tag{4.22}$$

Therefore, one gets

$$C_{\mathrm{DPS2}} = \frac{S_{\mathrm{eff}} \cdot p_9}{(p_{10} - p_9)} \tag{4.23}$$

$$= (3.46 \pm 1.23) \cdot 10^{-2}\,\frac{\mathrm{L}}{\mathrm{s}} \tag{4.24}$$

which is in agreement with the geometric value (table 4.1). The error is relatively large as the pressure reading p_9 only has an accuracy of ±30 %.

Table 4.1: **Comparison of geometric and measured conductance** of differential pumping section 2.

	Geometrical (L/s)	Experimental (L/s)
Conductance	$4.11 \cdot 10^{-2}$	$3.46 \pm 1.23 \cdot 10^{-2}$

4.3 Conductance of the butterfly valve

- **Geometrical conductance:**
  If the butterfly valve is fully open ($\alpha = 90°$), the conductance for a disc with a negligible small thickness is

$$C_{\mathrm{bf}} = \frac{A}{4} \cdot \bar{c} \tag{4.25}$$

where A is the area of the opening and $\bar{c}$ the average speed of the xenon atoms. The average speed $\bar{c} = 217.426$ m/s is valid for room temperature. If the valve is partially closed, A is reduced by the vertical projection of the slanted disc into the opening plane. A_{eff} then is

$$A_{\mathrm{eff}} = A \cdot (1 - \cos\alpha) = \pi r^2 \cdot (1 - \cos\alpha) \tag{4.26}$$

with the diameter r and the opening angle α defined in figure 4.4. Then one gets

$$C_{\mathrm{bf}}(\alpha) = \frac{\pi r^2}{4} \cdot \bar{c} \cdot (1 - \cos\alpha). \tag{4.27}$$

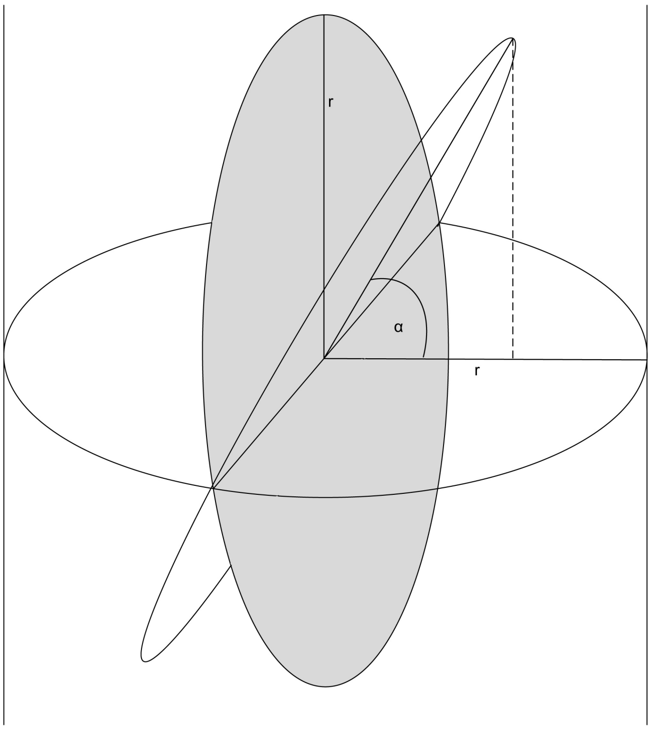

Figure 4.4: **Schematic sketch.** This schematic sketch shows the geometric dimensions of the butterfly valve. The area of the opening is $A_{\text{eff}} = \pi r^2 \cdot (1 - \cos\alpha)$

- **Measurement of the conductance:**
  To find the conductance experimentally, one calculates the flow through the butterfly valve q_{bf} and the flow through the second differential pumping section DPS2 q_{DPS2}. These two flows are supposed to be equal since there is no gas flow in other directions. The flow through the butterfly valve is given by the effective pumping speed of the turbo molecular pump S_{eff} in the main chamber and the pressure in the main chamber p_9

  $$q_{\text{DPS2}} = q_{\text{bf}} = S_{\text{eff}} \cdot p_9. \tag{4.28}$$

  The effective pumping speed is given by the pumping speed of the pump and the conductance of the butterfly valve C_{bf} which depends on the opening angle α:

  $$S_{\text{eff}} = \frac{C_{\text{bf}}(\alpha) \cdot S}{C_{\text{bf}}(\alpha) + S}. \tag{4.29}$$

  The flow q_{DPS2} is determined by the conductance C_{DPS2}.

  $$q_{\text{DPS2}} = C_{\text{DPS2}} \cdot (p_{10} - p_9). \tag{4.30}$$

If $q_{\mathrm{bf}} = q_{\mathrm{DPS2}}$, then

$$C_{\mathrm{bf}}(\alpha) = \frac{S \cdot C_{\mathrm{DPS2}} \cdot (p_{10} - p_9)}{S \cdot p_9 - C_{\mathrm{DPS2}} \cdot (p_{10} - p_9)}. \tag{4.31}$$

In figure 4.5, the geometrical and the measured conductances are shown for different degrees of opening. Again the accuracy of the experimental value is drastically limited by the pressure reading p_9.

Within the error bars, the geometrical and the experimental value only coincide for small and large opening angles. That is because the overall behaviour of the two values is different. The slope of the experimentally derived conductance decreases for large opening angles which contradicts the theory. The geometrical model which has been assumed might be too simple to be able to explain the flow through the butterfly valve. It is therefore not entirely correct to assume the projection of the disc in the opening area as an obstacle for the flow. On the contrary, molecules might glide over the slanted butterfly disc and not be stopped by it.

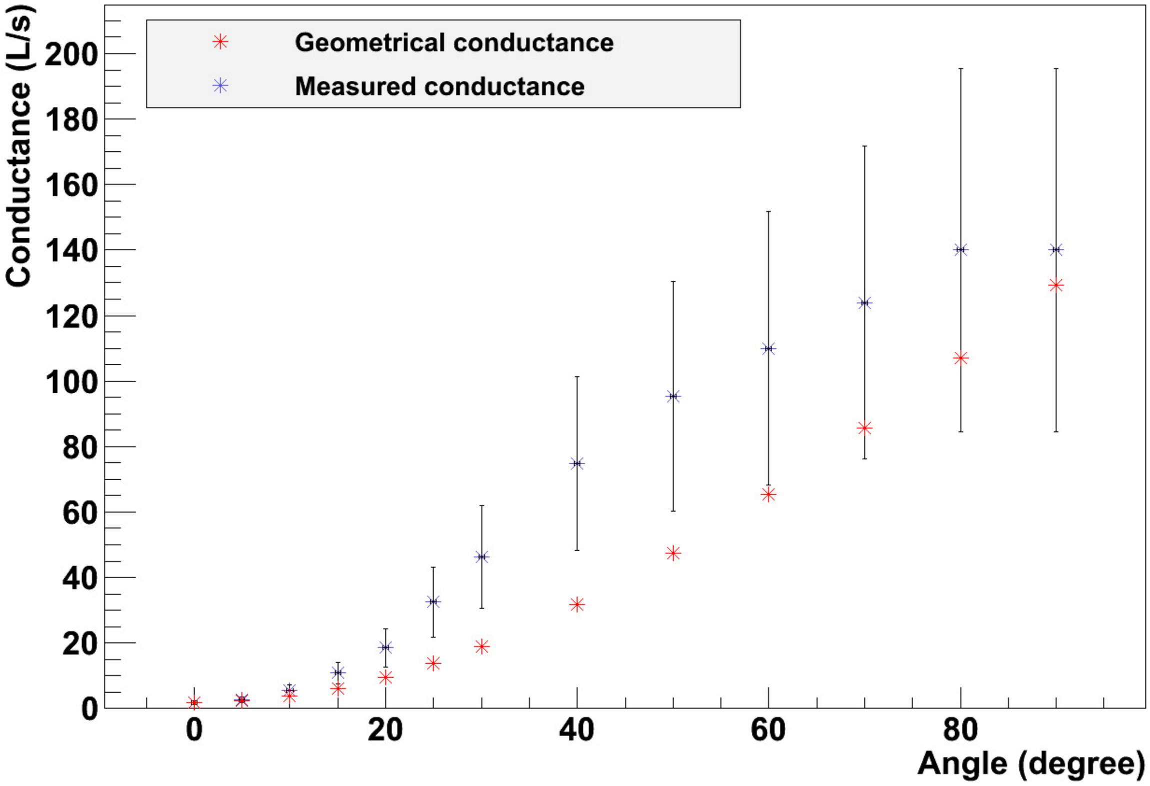

Figure 4.5: **Conductance of the butterfly valve.** The experimental and the geometrical value only coincide for small and large angles.

CHAPTER 5

Analysis of mass spectra

In this section, the mass spectrometer is used to get further information about the system. First, the spectrum of the xenon atoms is taken to analyze the isotopic composition and the impact of the butterfly valve on the mass spectrum. Eventually, first tests to measure the krypton concentration in xenon are done.

5.1 Isotopic composition of xenon atoms

The measuring process for the xenon mass spectrum was the following: The cold trap was cooled down to the temperature of liquid nitrogen and the gas inlet was opened. Now the xenon froze in the cold trap. The pressure in the cold trap was $\approx 5\,\%$ above vapor pressure. In figure 5.1, the intensity of the xenon isotopes is plotted versus time. The steps in the diagram are due to closure and opening of the butterfly valve. At the beginning of the measurement, the butterfly was open. Then it was three times closed during 120 seconds to an opening angle of 15° and opened again.

After this measurement the gas inlet was closed. In about 1 minute the pressure in the cold trap reached vapor pressure. The pressure in the main chamber was constant then. Therefore, the intensity measured by the RGA should be constant too. In figure 5.2, the intensity is plotted versus time for this second part of the experiment. As before, the steps are due to the closure and opening of the butterfly valve.

Table 5.1 shows the natural abundance of the xenon isotopes in comparison to the ratios which are shown in figures 5.1 and 5.2[1]. The arithmetic mean of the current values is taken to determine the abundance. The error is one order of magnitude smaller than the last significant digit of the value itself and has therefore been neglected. The values are purified from background effects which have been recorded beforehand.

---

[1] ^{124}Xe and ^{126}Xe are not listed as they are only present in trace concentrations.

As it can be seen in table 5.1, the measured abundance of the xenon isotopes does not exactly coincide with the natural abundance. In particular, the most abundant isotope ^{132}Kr is only detected with a ratio of 25.8 %, 1.2 percentage point less than it should be. This could be an evidence for impurities in the xenon gas (chapter 5.3).

Table 5.1: **Abundance of xenon isotopes** [See74].

Isotope	Natural abundance (%)	Measured abundance (%)
^{128}Xe	1.9	2.3
^{129}Xe	26.4	26.9
^{130}Xe	3.9	4.3
^{131}Xe	21.2	20.9
^{132}Xe	27.0	25.8
^{134}Xe	10.5	10.5
^{136}Xe	8.9	9.0

5.2 Calibration of the butterfly valve

The same measurement as described above is used to investige the reproducibility of positions of the butterfly valve. Therefore, the butterfly valve has been set six times to an opening angle of 15°, three times when the gas inlet was open, three times when it was closed. After changing the position of the butterfly valve, the system needed about 20 seconds to reach its equilibirum state. The slope is not reflected in the evolution of the pressure in the main chamber. This behaviour has not yet been explained. However, it had already been detected in the test setup [Ket12].

To investigate the reproducibility of the butterfly valve, the current ratio of all xenon isotopes measured by the residual gas analyzer for the different position changes of the butterfly (from open to 15° closed) are calculated. A Gaussian distribution is expected as the error is statistical. The mean within the error bars is the same whether the gas inlet is open or closed. It is concluded that the butterfly valve behaves in the same manner independently on the gas inlet. The number of counts for each current ratio is plotted versus the current ratio in figure 5.3. The current ratio for the change of the butterfly from a fully open position to an opening angle of 15° is determined to

$$r_{15^\circ/90^\circ} = 7.57 \pm 0.30. \tag{5.1}$$

Hence the butterfly position can be changed with an accuracy of

$$\frac{\sigma}{r_{15^\circ/90^\circ}} = \pm 4\,\% \quad \text{(relative error)} \tag{5.2}$$

within the one 1σ confidence level. It can be assumed that the absolute error is comparable for all butterfly positions. This is an enormous gain of accuracy in comparison with the

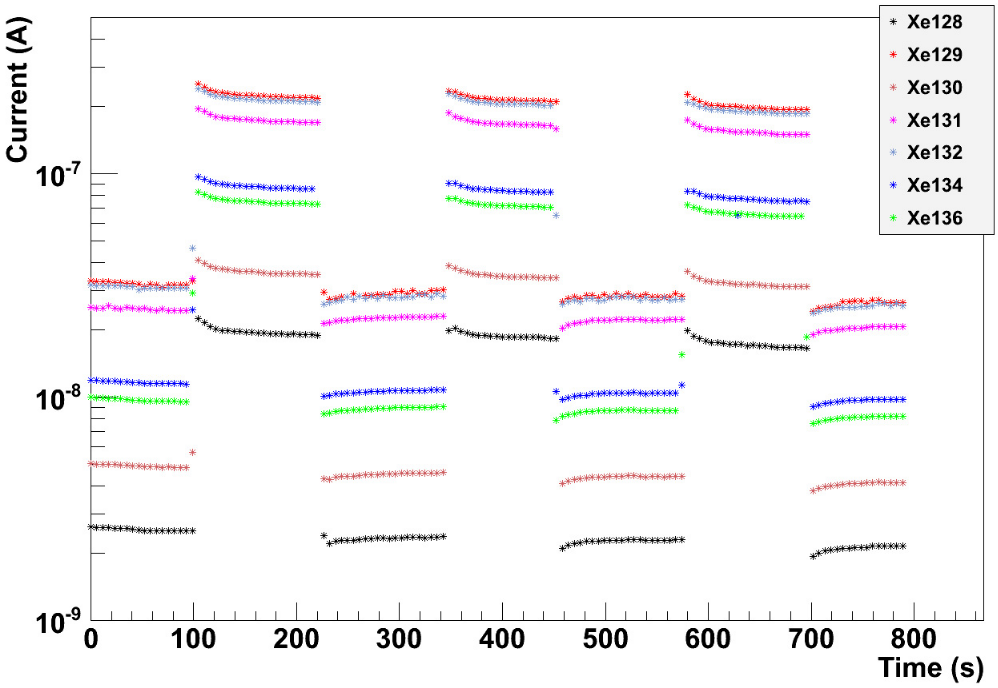

Figure 5.1: **Time evolution of xenon isotopes at two different butterfly positions (PV13 open).** In the diagram, the current measured by the RGA for different xenon isotopes is plotted versus time. The gas inlet is open. The steps in the diagram are due to position changes of the butterfly valve. It has been closed three times to an opening angle of 15° thereby resulting in a higher current and opened again.

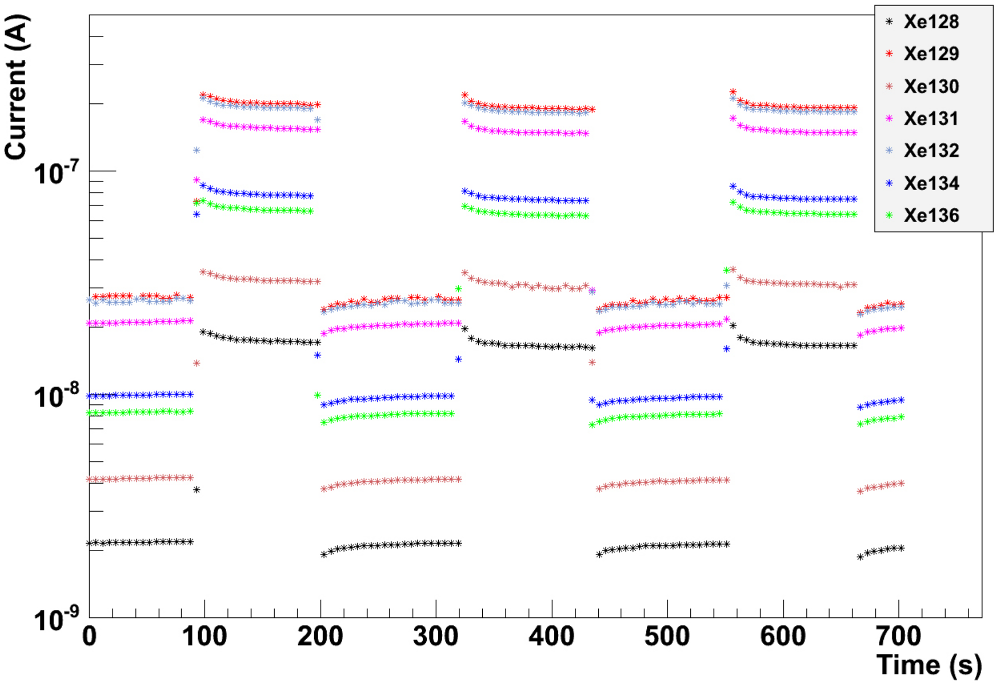

Figure 5.2: **Time evolution of xenon isotopes at two different butterfly positions (PV13 closed).** In the diagram, the current measured by the RGA for different xenon isotopes is plotted versus time. The gas inlet is closed.

test setup where the pressure in the main chamber and therefore the current in the RGA could be manipulated only very roughly.

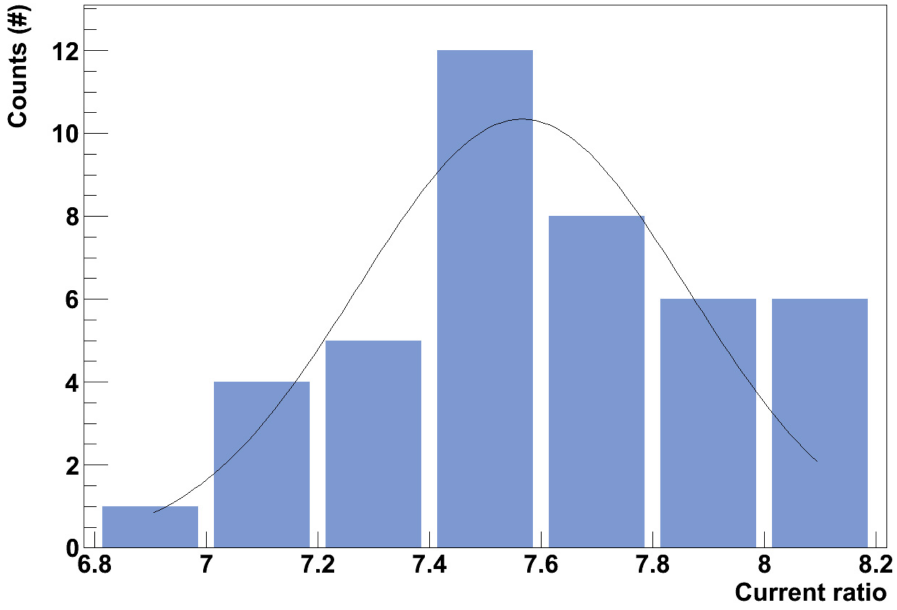

Figure 5.3: **Distribution of the current ratio** measured by the RGA when closing the butterfly from the fully open position to an opening angle of 15°. The ratios follow a Gaussian distribution.

5.3 Detection of krypton in xenon

In a last step of this bachelor thesis, it has been tried to use the setup as a detection system for the in situ krypton concentration in xenon gas which will later be its main application. Therefore, the spectrum has been measured with an opening angle of the butterfly of 15°. The results are shown in figure 5.4.

If the system was sensitive enough to detect krypton, the highest peaks should be at $m/z = 84$ as the isotopic krypton distribution in table 5.2 shows. The peaks of the other krypton isotopes should also be visible in the ratio of their abundance. However, this is not the case. Either they are not in the correct ratio ($m/z = 78$, $m/z = 81$) or the peaks are outweighed by other peaks in the neighbourhood (^{83}Kr, ^{84}Kr, ^{86}Kr) and almost get lost in the background signal. As the xenon peaks and other characteristic molecules (for example CO_2 at $m/z = 44$ in figure 5.5) appear in the right position, an offset of the mass to charge scale of the RGA can be excluded as a reason for this outcome. The highest peak in the krypton range is detected at $m/z = 85$ which indicates that only contamination in the system and no krypton is measured (there are only trace amounts of the isotope ^{85}Kr in xenon gas that is why there should not be at peak at $m/z = 85$). The high background

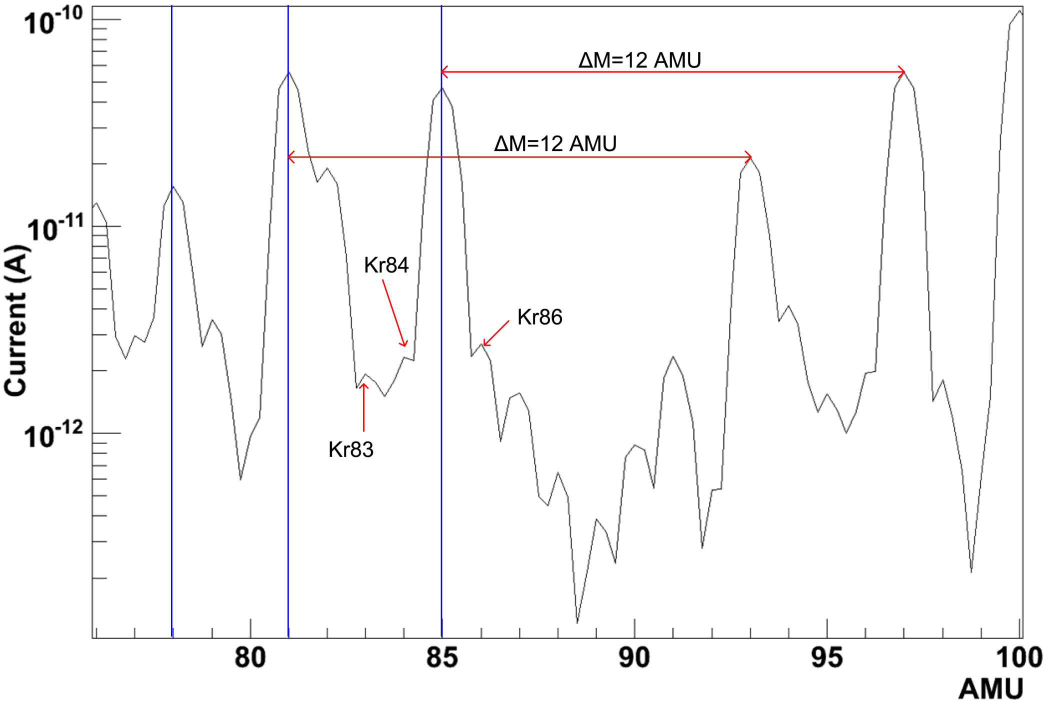

Figure 5.4: **Mass spectrum of the krypton range (butterfly 15° open).** The peaks of ^{83}Kr, ^{84}Kr, ^{86}Kr are very small compared to the peaks at $m/z = 78$, $m/z = 81$ and $m/z = 85$ which are associated with hydrocarbon background. This hypothesis is backed up by the distance of $\Delta M = 12$ to the next peak which is the mass of the most abundant carbon isotope.

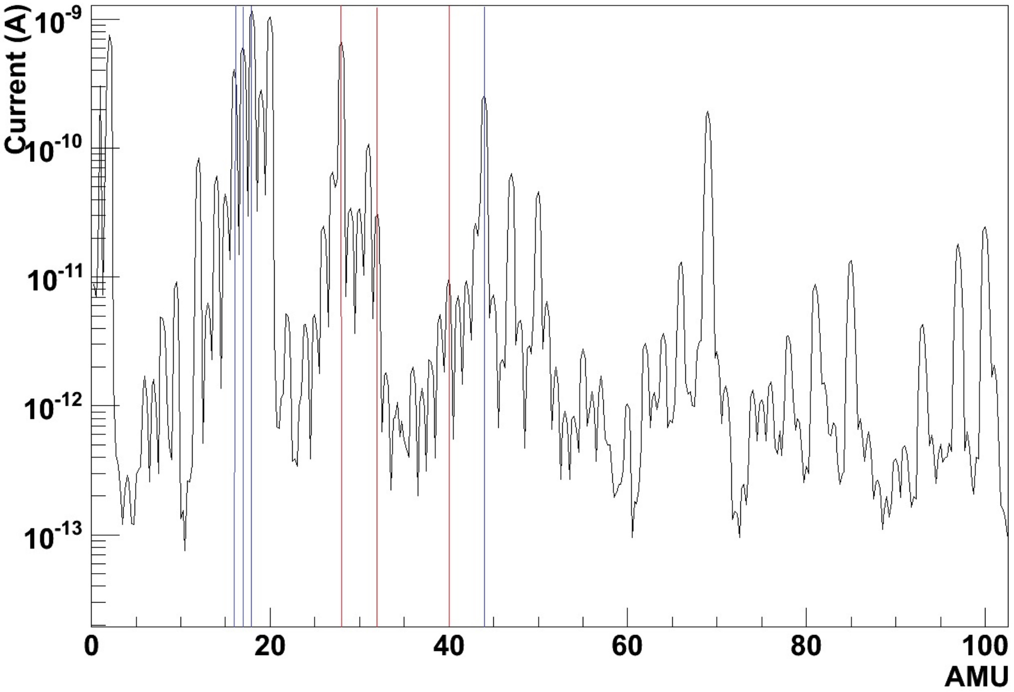

Figure 5.5: **Mass spectrum of the background.** Despite out-baking, a lot of impurities remained in the system, for instance CO_2 at $m/z = 44$, water at $m/z = 16$, 17 and 18 (blue lines) and air (nitrogen at $m/z = 28$, oxygen at $m/z = 32$, argon at $m/z = 40$; red lines). The whole background spectrum is shown in figure 5.6.

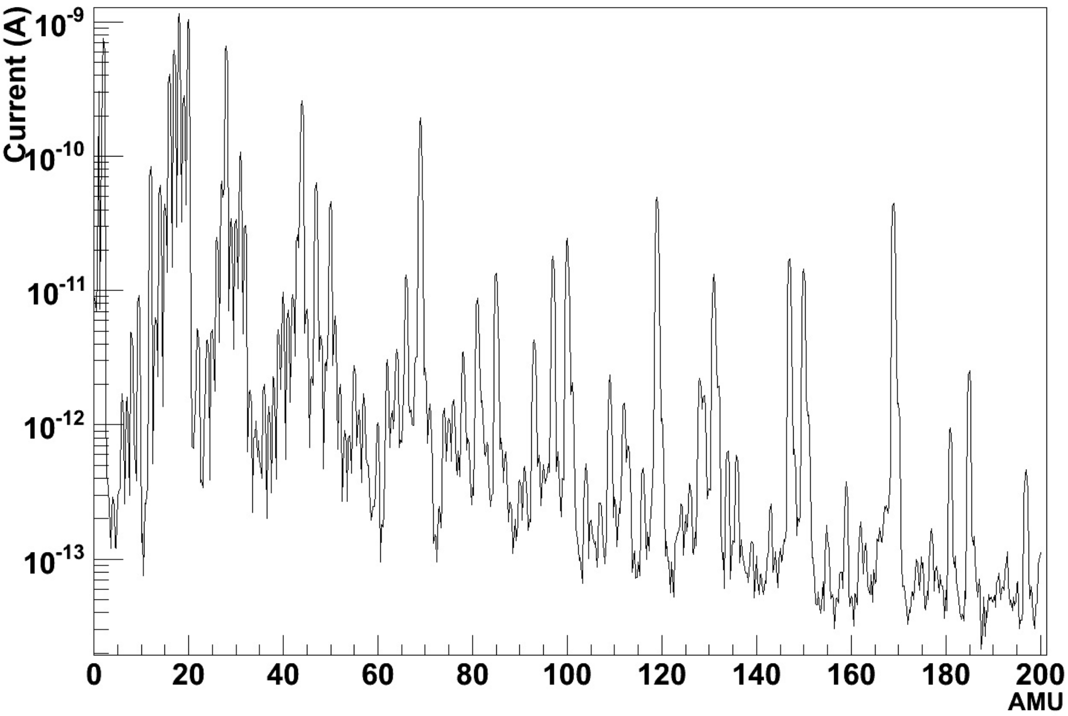

Figure 5.6: **Mass spectrum of the background** showing the whole mass range. In addition to the impurities discussed in figure 5.5, there are further impurities at higher masses which are very likely also due to hydrocarbon molecules.

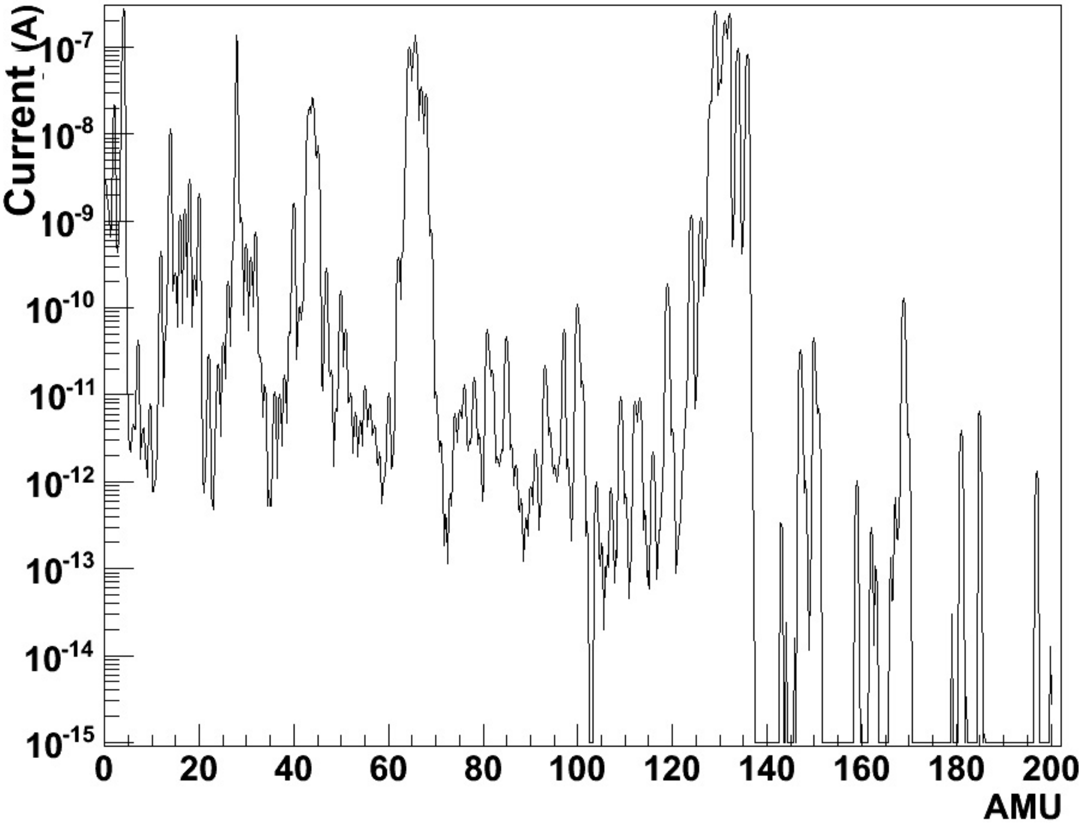

Figure 5.7: **Mass spectrum of the xenon gas.** The butterfly is 15° open. The spectrum shows the characteristic xenon peaks (single-ionized at $m/z = 128 - 136$, double-ionized at $m/z = 64 - 68$ and triple-ionized at $m/z \approx 42.5 - 45.5$.

contamination can be seen in figures 5.5 and 5.6.

Table 5.2: **Abundance of krypton isotopes** [See74].

Isotope	Natural abundance (%)
^{78}Kr	0.35
^{80}Kr	2.25
^{82}Kr	11.6
^{83}Kr	11.5
^{84}Kr	57.0
^{86}Kr	17.3

This contamination is very likely due to hydro-carbon molecules with the chemical structure $C_kH_lO_mN_n$. Organic structure can disintegrate when being ionized since electrons are necessary for the bindings [Gro04]. That makes it difficult to track these molecules in mass spectra.

One hint for the hypothesis of hydro-carbon contamination is the fact that peaks in the mass spectrum appear with a distance of $\Delta m = 12$ AMU (figure 5.1). This is the mass of the most abundant carbon isotope ^{12}C. This indicates carbon structures which have broken at different bindings. Possible candidates for the peaks in the krypton range are

- **$m/z = 78$:**
  C_6H_6, a benzene ring. Benzene is an aromate and a natural constituent of petroleum. Although the pumps of the system are oil free, oil might be present in the VAT valves[2]. For benzene the highest peak is expected at $m/z = 78$ (53 % of the concentration), minor peaks at $m/z = 50, 51, 52$ ($\approx 10\,\%$ for each peak) [Inf07]. These minor peaks might be outweighed by other impurities.

- **$m/z = 81$:**
  C_5H_5O, pyrylium salt, or C_5H_7N, 3-methyl-1H-pyrrole.

- **$m/z = 85$:**
  C_6H_{13}, a fragment of a linear alkane chain. Alkanes (saturated hydrocarbons) have the chemical structure C_nH_{2n+2}. If they break apart by ionization, molecule fragments with the formula C_6H_{13} can be formed.

Except for the benzene, there is no information in the Transpector 2 manual about the mass spectra of the mentioned hydrocarbons.

It can be concluded that the system is not yet sensitive enough for the detection of the in-situ krypton concentration in xenon gas. Possible enhancements to increase the sensitivity are discussed in chapter 6.

---

[2] Benzene was probably also present present in the test setup [Ket12].

CHAPTER 6

Summary and outlook

The RGA/cold trap detection system has been installed at the main setup in the XENON laboratory in Münster and has been tested. However, further work needs to be done to use it for krypton detection in xenon.

The main purpose of this bachelor thesis, to provide reproducible conditions for the krypton detection in the setup, has been reached. By analyzing the gas flow in the system, it was shown that for an inlet pressure up to 2 bar, conditions are reproducible. Comparing the measured gas flows with theoretical values, there is good agreement. Thus the gas flow in the system is well understood.

The butterfly valve constitutes a special improvement compared to the test setup as it allows a reproducible control of the pressure in the main chamber. The current ratio measured by the RGA when closing the butterfly valve from the fully open position to an opening angle of 15° has been determined to $r_{15°/90°} = 7.57 \pm 0.30$. It can be assumed that the absolute error is similar for the other butterfly positions.

A possible enhancement of the system consists in using a longer capillary for the differential pumping section 1 as for high inlet pressure of the xenon gas, vapor pressure in the cold trap is not yet fully reached.

It has not been possible so far to determine the sensitivity of the setup and to measure krypton in pure xenon gas. One reason for this is the high contamination by hydrocarbons which could be proven by a discussion of the mass spectrum. Leak-checking of the whole system is needed to reduce this background. It is very likely that internal leaks constantly contaminate the pure xenon gas which is in the system. Although the system has already been baked out, this should be repeated. Especially the main chamber should be baked out during longer time in order to reduce impurities in the setup.

However, the sensitivity of the system is not only limited by the concentration of impurities but also by the flow rate into the system. A spiral cold trap with a higher surface inside the liquid nitrogen would probably guarantee that all the xenon gets frozen when increasing the inlet pressure and thereby the flow rate.

For a calibration of the system in order to get absolute values of the krypton concentration in the measured xenon gas and to find out the sensitivity of the setup, a doping method has to be employed. This means that the xenon gas is doped with known amounts of krypton, each time decreasing the krypton to xenon ratio. From the evolution of the current signal of the different krypton isotopes for different doping strengthes, one can infer the sensitivity of the RGA/cold trap setup.

These measurements could not be realized in the frame of this bachelor thesis. They are a project for further investigation in order to establish the RGA/cold trap method as an user-friendly stand-alone analyzer of trace amounts of rare gases in xenon.

Bibliography

[Abe11] K. Abe, *et al.* “Distillation of Liquid Xenon to Remove Kypton”. `arXiv:0809.4413v3`.

[Agl98] M. Aglietta, *et al.* “Muon ‘depth-intensity’ relation measured by the LVD underground experiment and cosmic-ray muon spectrum at sea level”. *Physical Review D* 58 (November 1998).

[Apr10a] E. Aprile and L. Baudis. “Liquid noble gases”. *Particle Dark Matter*. Ed. G. Bertone. New York: Cambridge University Press, 2000. 413-436.

[Apr10b] E. Aprile, *et al. XENON1T at LNGS. Technical Design Report.* 2010.

[Apr12a] E. Aprile, *et al.* “Analysis of the XENON100 Dark Matter Search Data”. `arXiv:1207.3458v1`.

[Apr12b] E. Aprile, *et al.* “The XENON100 Dark Matter Experiment”. `arXiv:1107.2155v2`.

[Apr12c] E. Aprile, *et al.* “Dark Matter Results from 225 Live Days of XENO100 Data”. `arXiv:1207.5988v1`.

[Beg91] K. G. Begeman, *et al.* “Extended rotation curves of spiral galaxies – Dark haloes and modified dynamics.” *Monthly Notices of the Royal Astronomical Society* 249 (April 1991): 523-537.

[Bon64] A. Bondi. “Van der Waals Volumes and Radii.” *The Journal of Physical Chemistry* 68 (1964): 441-451.

[Che99] C. Y. Chen, *et al.*. “Ultrasensitive Isotope Trace Analyses with a Magneto-Optical Trap”. *Science* 286 (1999) 1139.

[Dem10] W. Demtröder. *Experimentalphysik 3.* Berlin: Springer, 2010.

[Dob11] A. Dobi, *et al.* “Detection of krypton in xenon for dark matter applications”. `arXiv:1103.2714v4`.

[Gro04] J. Gross. *Mass Spectrometry. A textbook.* Berlin: Springer, 2004.

[Gru64] A. Grütter and J.C. Shorrock. “Vapour Pressures of Xenon (77°-180° K) and Krypton (77°-130° K)”. *Nature* 204 (December 1964): 1084-1085.

[Inf07] Inficon. *Transpector2. Operating Manual.* 2007.

[Jou06] K. Jousten (Ed.). *Wutz Handbuch Vakuumtechnik.* Wiesbaden: Vieweg, 2006.

[Jun96] G. Jungman. *et al.* “Supersymmetric Dark Matter”. *Physics Reports* 267 (1996): 195-373.

[Ket12] H. Kettling. *Trace Gas Analysis of Krypton for the XENON Dark Matter Project.* Münster: Westfälische Wilhelms-Universität, 2012.

[Nis11] NIST. *NIST Chemistry WebBook*. 2011.

[Ost03] J.P. Ostriker and P. Steinhardt. “New Light on Dark Matter”. *Science* 20 (June 2003): 1909-1913.

[Pol64] G. Pollack. “The Solid State of Rare Gases”. *Review of Modern Physics* 36 (1964): 748791.

[Rei10] P. Reineker and M. Schulz. *Theoretische Physik V. Statistische Physik und Thermodynamik.* Weinheim: Wiley-VCH, 2010.

[See74] W. Seelmann-Eggebert, *et al. Karlsruher Nuklidkarte.* Karlsruhe: Gesellschaft für Kernforschung, 1974.

Eigenständigkeitserklärung

Hiermit versichere ich, dass ich die vorliegende Arbeit selbständig verfasst und keine anderen als die angegebenen Hilfsmittel benutzt habe. Die Stellen der Arbeit, die dem Wortlaut oder dem Sinn nach anderen Werken entnommen sind, wurden unter Angabe der Quelle kenntlich gemacht. Das gilt auch für Zeichnungen und andere Darstellungen.